Mechanical response of a novel hybrid tube composed of an auxetic outer layer

Krishna Prasath Logakannan[1,2], Jayaganthan Rengaswamy[3], Shanmugam Kumar[4], Velmurugan Ramachandran[2] and Dong Ruan[1,*]

[1] School of Engineering, Swinburne University of Technology, Hawthorn, VIC 3122, Australia

[2] Department of Aerospace Engineering, Indian Institute of Technology Madras, Chennai 600036, India

[3] Department of Engineering Design, Indian Institute of Technology Madras, Chennai 600036, India

[4] James Watt School of Engineering, University of Glasgow, Glasgow G12 8LT, UK.

*Corresponding author. Email: druan@swin.edu.au

Abstract

In this study, the deformation and energy absorption of a novel hybrid tube is investigated both experimentally and numerically. The architecture of the proposed hybrid tube composed of an inner conventional tube and a co-axially arranged outer auxetic tube. Quasi-static compressive tests were conducted on the auxetic tubes, the conventional tubes and the hybrid tubes, respectively. A three-dimensional digital image correlation technique was used to monitor the evolution of radial contraction of the tubes. Measured performance of the tubes were compared in terms of force, energy absorption, and specific energy absorption. Finite element (FE) models were also developed for the three types of tubes, analyzed using ANSYS/LS-DYNA, and validated by experimental measurements. Both experimental and numerical results showed that the presence of the auxetic tube in the hybrid tube alters the deformation mode of the conventional tube by exerting a radial force. Parametric studies were performed to investigate

the effects of the outer auxetic tube, wall thickness of the inner conventional tube, the failure strain, and yield strength of the outer tube material on mechanical performance of the hybrid tube. Increasing the yield strength of the outer auxetic tube improved both the energy absorption and specific energy absorption of the hybrid tube significantly.

Keywords: Axial compression; Auxetic tube; Hybrid tube; Energy absorption; Crashworthiness.

1. Introduction

Lightweight cellular structural materials are gaining enormous attention due to superior properties specific stiffness, strength, and toughness [1, 2]. There are several classes of cellular materials, one such class is referred to as “auxetics”. “Auxetics” is the term coined for the cellular structures with negative Poisson’s ratios. These structures expand laterally under axial tensile loading and contracts laterally under axial compressive loading. Researchers have developed various auxetic geometries, and some representative auxetic unit cells geometries are discussed as follows. Grima and Evans [3] created a structure with rotating rigid square unit cells which exhibits auxetic behavior. Grima et al. [4] and Grima and Gatt [5] also developed other types of auxetic structures by connecting stars and perforating sheets. Gaspar et al. [6] designed a novel honeycomb which exhibits auxetic behavior. Bertoldi et al. [7] achieved a negative Poisson’s ratio in a structure through elastic instability of an array of circular holes. Under compression, the circular holes transformed to mutually orthogonal ellipses when the strain was beyond a critical magnitude, which resulted in a negative Poisson’s ratio. Shen et al. [8] used the concept of elastic instability to form a three-dimensional auxetic structure. Li et al. [9] developed an auxetic structure with alternative indents on vertical ribs,

which possessed good elastic properties. Different auxetic structures were reviewed in [10] and their applications were summarized [11, 12]

Tubes offer superior properties such as lightweight, high stiffness, strength, and energy absorbing capability. Detailed experimental studies [13] have been conducted to examine the influence of the circular tubes' diameter, height, and wall thickness on their deformation mode and load carrying capacities. Holes in the walls of the tubes influences their deformation behavior to a great extent. Baaskaran et al. [14] introduced elliptical cut-outs in circular thin-walled tubes and found that the location of cutouts drastically changed the deformation mode and energy absorption of the thin-walled tubes. When the two cut-outs were positioned on opposite faces, a transition of collapse modes from concertina to diamond modes to completely diamond mode was observed. Bodlani et al. [15] studied the crushing of mild steel square tubes with a different number of holes and spacing between them. They found that the position of the holes was very crucial for triggering progressing collapse.

Efforts have been made to enhance the mechanical performance of tubes by introducing hybrid tubes. One such an approach is inserting lightweight materials such as foams (conventional or auxetic) and honeycombs inside the tube [16–21], and another approach is wrapping tubes externally by additional materials [22] or employing two tubes [23–27]. Examples of the first approach include the work by Hussein et al. [16] who studied the mechanical response of honeycomb and foam filled aluminum square tubes and reported an increase in specific energy absorption (SEA) of such hybrid tubes. Liu et al. [18] studied axial crushing of carbon fiber reinforced polymer (CFRP) tube with aluminum honeycombs in it. Introduction of honeycombs improved SEA of the tube; however, it was depended on the geometry of the honeycomb. Mohsenizadeh et al. [20] filled a square aluminum tube with an auxetic foam and studied the compressive properties of the hybrid tube. They reported 18% and 6% increase in SEA for the auxetic foam filled tube when compared with the empty tube

and the tube filled with a conventional foam, respectively. Hou et al. [21] studied the crushing response of auxetic foam filled square, circular, and conical shaped tubes and also investigated the effect of Poisson's ratio of the foam on the force and deformation of each tube. Their single objective optimization revealed that optimal Poisson's ratios of the foam to achieve the maximum specific energy absorption was -0.62 for square and circular tubes and -0.60 for conical tube.

For the second approach, Hussein et al. [22] wrapped carbon fiber composite tube by aluminum sheets and observed varied deformation modes. Shin et al. [23] investigated axial crushing and bending of aluminum/glass fiber reinforce polymer (GFRP) square tubes. They reported that hybrid tube with 90° ply orientation exhibited better energy absorption capability under axial crushing. Sharifi et al. [24] studied the energy absorption of two circular tubes arranged coaxially. They found that such bi-tubal tube was better than the equivalent monotube in terms of crashworthiness. The effects of gap between two tubes, tube's wall thickness, tube's length, and grooves on the tube were also examined. Reuter and Tröster [25] found that the SEA of hybrid aluminum/CFRP tube was greater than that of the aluminum tube. Sun et al. [26] investigated the effects of filament winding angle and the number of layers on the performance of aluminum/CFRP hybrid tubes. They reported that the energy absorption of the hybrid tube was better than the sum of that of aluminum and CFRP tubes. Zhu et al. [27] studied the performance of aluminum/CFRP hybrid tubes with three different configurations, namely aluminum tube outside and CFRP tube inside, CFRP tube outside and aluminum tube inside, and two aluminum tubes (inside and outside) with CFRP tube in between. The configuration with aluminum tube outside and CFRP tube inside exhibited better SEA than the other two configurations. Wang et al. [28] reported that the SEA of aluminum/CFRP hybrid tube increased with the increase in wall thickness of the CFRP tube.

A few studies were conducted on the performances of auxetic tubes. Lee et al. [29] developed a cellular tube with re-entrant shaped voids on it and another tube with hexagonal honeycomb voids. The designed tubes were manufactured from stainless steel 316L using selective laser melting process, and they were crushed using a moving mass cart. Deceleration of the auxetic tube was steady, whereas it oscillated in the honeycomb tube. Karnessis and Burriesci [30] investigated local buckling of an auxetic tube (re-entrant based tube) under bending. They found the geometrical parameters affected the kinking resistance of tubes. Ren et al. [31] studied auxetic tube based on elastic instability mechanism. They found that the array of circular holes did not generate auxetic behavior for copper tubes. They performed an eigenvalue analysis on a tube with circular holes and found that an array of mutually orthogonal ellipses could produce auxetic behavior. Recently Zhang et al. [32] developed a novel auxetic tube in which the wall of the tube had internal holes along the circumference which collapsed through elastic instability. Bhullar et al. [33] developed biocompatible auxetic stent made of poly-caprolactone through electrospinning and micromachining. Another study [34] proposed an auxetic tube which could generate rotary motion through axial compression. A detailed review [35] on the design, fabrication and applications of different auxetic tubes is published recently. To the best of authors' knowledge, no investigation on hybrid tubes with an auxetic tube as the outer layer has been reported so far. Under compression, the outer auxetic tube contracts and may change the deformation, load carry capacity, and energy absorption characteristics of the inner conventional tube.

In this work, a novel architecture of a hybrid tube composed of a conventional inner tube and a co-axially arranged auxetic outer tube is proposed and its enhanced energy absorption characteristics is demonstrated. Quasi-static uniaxial compressive tests are conducted on auxetic tubes, conventional tubes, and the hybrid tubes and their deformation are captured using three-dimensional digital image correlation (3D DIC). Moreover, finite element (FE) models

are developed for all the three types of tubes and analyzed using ANSYS/LS-DYNA solver. The numerical results are compared with the experimental results for validation. Furthermore, the effects of the auxetic tube, conventional tube's wall thickness, failure strain, and yield strength of the outer auxetic tube material on the deformation, damage, and energy absorption behavior of hybrid tube are discussed.

2. Hybrid tube design, material properties and test setup

2.1. Design and fabrication of auxetic and hybrid tubes

Auxetic behavior can be achieved via different mechanisms, as discussed in the Introduction. The auxetic tube used in this work is based on the instability of an array of mutually orthogonal elliptical holes proposed by Ren et al. [31]. The reason for selecting this pattern (with mutually orthogonal elliptical holes shown in Fig. 1) was the ease of manufacturing – this pattern can be generated by conventional manufacturing technique at a low cost.

The novel hybrid tube concept proposed in this work is shown in Fig. 2. An auxetic tube is placed outside a conventional tube, concentrically, in such a way that the inner diameter of the auxetic tube is almost same as the outer diameter of the conventional tube. Both the tubes are of the same height. This tubular arrangement is termed as the hybrid tube in this work. Under uniaxial compression, the outside auxetic tube shrinks in the radial direction (i.e. shrinks in diameter) and exerts a force on the outer surface of the inner conventional tube. This force may change the deformation mode and enhance the load and energy absorption characteristics of the inner conventional tube.

All the tubes studied in the experiments were made of extruded aluminum alloy 6060 with T5 heat treatment and were supplied by the same manufacturer. The height of all tubular samples was 100 mm. The conventional tubes were cut from a tube of 44 mm outer diameter

and 1.5 mm wall thickness. The auxetic tubes were fabricated from a tube with 50 mm outer diameter and 3 mm wall thickness. The above-mentioned dimensions were design value; however, the average measured dimensions of the procured tubes are listed in Table 1. It should be noted that there was a gap of approximately 0.28 mm between the inner surface of the outer auxetic tube and the outer surface of the inner conventional tube.

Mutually orthogonal elliptical holes (Fig. 1) were cut on commercially available monolithic tubes using conventional machining approach. The dimensions of the elliptical holes are shown in Table 2. A pair of holes is defined as a combination of a horizontal and a vertical elliptical hole (highlighted in the yellow box in Fig. 1). In order to ensure symmetry in both the circumferential and longitudinal directions, six pairs of holes around the circumference and four pair of holes along the longitudinal direction were cut to fabricate auxetic tubes. Please note if tubes are expected to have good corrosion and fire resistance, care should be taken when introducing holes which may affect the corrosion and fire resistance of tubes.

Four conventional and auxetic tubes were fabricated. Two conventional and auxetic tubes were assembled into two hybrid tubes. Therefore, two samples were prepared for each of the three types of tubes, i.e. auxetic, conventional, and hybrid, as shown in Fig. 1.

2.2. Material properties

To obtain the material properties of tubes, tensile test coupons were cut from 50 mm diameter tube and tested according to AS 1391 – 2007 standard (Fig. 3a). Since both the tubes (with diameters of 50 mm and 44 mm) were made of the same alloy and supplied by the same manufacturer, their properties are assumed to be the same. Stress-strain curves obtained from the quasi-static tensile tests are shown in Fig. 3(b). The elastic region of the stress-strain curve is quite reproducible, while slight discrepancies in flow stress and failure strain are observed.

2.3. Axial compressive tests of tubes

Quasi-static axial compressive tests of the tubes were carried out on a 50 kN and 1 MN MTS machines. Tubes were placed between two platens, the bottom platen was fixed, and the top platen was moved downwards at a constant speed of 10 mm/min [13]. Two repeated compressive tests were conducted on each of the conventional, the auxetic, and the hybrid tubes. Force and displacement were recorded by the MTS machine. The images were captured using a 3D DIC system and surface strain evolution of the auxetic tubes and the hybrid tubes were evaluvated. Two cameras were set up at a certain distance and calibrated before the tests (Fig. 4). These two cameras captured almost a quarter of the outer circumference of the tubes. Recorded images were processed using a commercial software named Vic-3D supplied by Correlated Solutions®. Test details are summarized in Table 1.

3. Finite Element Modelling

Finite element (FE) models for the conventional, auxetic, and hybrid tubes were developed using ANSYS/LS-DYNA. The auxetic tube was modelled according to the fabricated dimensions in SOLIDWORKS, imported into LS-PrePost and meshed with solid elements (ELFORM = 1) of 0.75 mm. A mesh convergence test was conducted and confirmed a converged result at this mesh size. The conventional tube was modelled and meshed using TSHELL elements of ELFORM = 5 in LS-Prepost. The gap between the outer tube and inner tube (mentioned in Section 2.1) was also modelled. Meshed tubes were compressed between two rigid platens (top and bottom). All degrees of freedom (DOF) of the bottom platen were fixed. The top platen was free to move in the crushing direction, while the other five degrees of freedom were fixed. To reduce the computational time, the top platen was set to move at a speed of 400 mm/s, faster than that of it in the experiments. To ensure that such increase in speed did not introduce significant dynamic effects, the ratio of kinetic energy to internal

energy is continuously monitored, and the maximum value of it was less than 0.1% in the entire crushing process. Therefore, the higher speed used in the FE models was deemed reasonable.

*CONTACT_AUTOMATIC_SURFACE_TO_SURFACE was set up between the rigid platens and the tubes. The static friction coefficient of 0.25 was determined using a slip test between the tubes and the compression test platens. *CONTACT_AUTOMATIC_GENERAL was set up for the auxetic tube, and *CONTACT_AUTOMATIC_SINGLE_SURFACE was set for the conventional tube and the hybrid tube simulation. To obtain the reaction forces, *FORCE_TRANSDUCER_PENALTY was used whenever single surface contact was employed in the model. *CONTACT_AUTOMATIC_SURFACE_TO_SURFACE was set for the interaction between the inner conventional and the outer auxetic tubes in a hybrid tube. Appropriate hourglass control was introduced for all three models.

Material properties used in the FE models were obtained from the tensile tests of coupons (Fig. 3). *MAT_MODIFIED_PIECEWISE_LINEAR_PLASTICITY was used for all tubes. Since failure was observed in the experiments for both the auxetic and hybrid tubes, a failure criterion was employed in their FE models. Parts of the tubes reaches complex stress states and it is well known that failure strain from uniaxial tensile tests does not work well for such complex stress state, a triaxiality based failure criterion was introduced to simulate the failure in the auxetic and the hybrid tubes. Fracture locus of the material (aluminum alloy 6000 series with heat treatment) was obtained from the literature [36], and shown in Fig. 5. Failure strain versus triaxiality curve was provided as input, and GISSMO damage model was activated by setting IDAM=1 in *MAT_ADD_EROSION. No failure criterion was set for the conventional tubes because no failure was observed in the corresponding experimental tests.

4. Results

4.1. Conventional tubes

Under quasi-static compression, these tubes exhibited axisymmetric deformation mode with six lobes. It can be seen from Fig. 6 that the exact same number of lobes are observed in the finite element analysis (FEA). Force-displacement curves obtained from the experiments and the FEA are shown in Fig. 7. Two repeated experimentally measured force-displacement curves are almost identical. Moreover, the force-displacement curve obtained from the FEA matches reasonably well with the experimental results in terms of force. The discrepancy is observed in displacements where the peak forces appear. This is mainly due to the larger displacement at which the first force valley present in the FEA, which is due to the length of the first lobe in the FEA is slightly larger than that in the experiments. The average initial peak forces from the experiments and FEA are 40.0 kN and 40.2 kN, respectively. After the initial peak, fluctuation in force is observed in both the experiments and the FEA, which corresponds to the formation of the lobes. Mean force is the average value of force in the displacement ranged from 10 mm to 70 mm. The average mean force obtained from the experiments and FE model is 21.4 kN and 20.8 kN, respectively, with a difference of less than 3%. This indicates that the FE model is able to predict the deformation mode and force values for conventional tubes.

4.2. Auxetic tubes

Two experimentally tested auxetic tubes exhibited the same deformation behavior. Figure 8(a) shows the deformation of one auxetic tube (Sample 1) observed from the experiment at various displacements. Elliptical holes start to collapse (Point ① in Fig. 8a) at a displacement of 2.5 mm. An initial peak force is observed at this point (Point ① in Fig. 8b). The bottom part of the tube starts to shrink first, as seen at Point ② of Fig. 8(a). Subsequently, the entire auxetic tube shrinks at Point ③ (Fig. 8a). During this process, the force value remains almost constant with a small kink at Point ② shown in Fig. 9. Beyond Point ③, the bottom

layer of the tube (in the yellow box) deforms locally as shown at Point ④ of Fig. 8(a). This deformation leads to an increase in the force between Points ③ and ④ in Fig. 9. Cracks form at weak points and cause a sharp drop in the force between Points ③ and ④. One such weak point is highlighted (in the yellow box) at Point ③ of Fig. 8(a). The same deformation is observed at the top layer between Points ④ and ⑤. However, it is not visible in Fig. 8(a) because the top platen hinders the view. After Point ⑤, force starts to increase again. The middle portion of the tube starts to expand at a displacement of 43 mm, and cracks start to form at a displacement of 45 mm. Fractured tube at a displacement of 50 mm is shown at Point ⑥ of Fig. 8(a). The middle portion of the auxetic tube carries the load before failing, as it can be seen in Fig. 9 (between Points ⑤ and ⑥). A small drop in the force between Points ⑤ and ⑥ is due to the rearrangement of the voids before the expansion of the middle portion. The deformation mode obtained from the FEA of the auxetic tube are shown in Fig. 8(b). Similar deformation mode has been observed in the experiments and FEA.

The comparison of the force-displacement curves obtained from the experiments and the FEA of the auxetic tube is shown in Fig. 9. The initial peak force obtained from the FEA of the auxetic tube is 5.6 kN, which is very close to the averaged peak force obtained from the experiments of the two samples (5.4 kN). After this initial peak, all the experimental and FEA curves match very well up to a displacement of approximately 19 mm. Beyond this point, although both the numerically simulated and experimentally measured forces have three peaks, the numerically simulated force is less than that in the experiments, which might be due to the higher frictional coefficient between inner surface of the tube and platen in the experiments. Moreover, kinematic hardening of the material during the complex folding could also play a part, which was not considered in the current FE model. The drop in force occurred at a displacement of approximately 45 mm in both the FEA and experiments, which corresponds to the complete failure of the tube.

The amount of radial contraction of the auxetic tube was measured using 3D DIC system described in Section 2.3. The magnitude of radial contraction was calculated as follows. As shown in Fig. 1 that the XZ-plane is the cross-sectional plane of the auxetic tube, thus the displacement values along the X and Z directions are used to calculate the magnitude of radial contraction of the auxetic tube. Figure 10 shows the magnitude of radial contraction obtained from the DIC and the FEA of the auxetic tubes. As stated before, only a quarter of the tube was covered well by the DIC cameras, and the calculated portion is shown in Fig. 10(a). At an axial displacement of 10 mm, the radial contraction (radius) observed at the bottom portion of the auxetic tube is approximately 4 mm whereas the radial contraction at the top portion of the auxetic tube is approximately 2 mm. The same values of radial contraction are observed in the FEA as well (Fig. 10b). The tube completely shrinks at a displacement of 20 mm. The maximum radial contraction obtained from both the experiments and the FE model is approximately 5 mm.

4.3. Hybrid tubes

Figure 11 shows the experimentally and numerically observed deformation mode of the hybrid tube. Although two samples were prepared, one sample was accidentally damaged in the test. Therefore, only one sample was successfully tested. Under axial compression, the outer auxetic tube did not exhibit any radial contraction due to the strong resistance of the inner conventional tube. At a displacement of 2.8 mm, a crack initiate in the outer auxetic tube. The crack developed in the auxetic tube at a displacement of 4.5 mm is highlighted in the yellow box at Point ① of Fig. 11. The corresponding force values are shown in Fig. 12. Several cracks form in the outer auxetic tube after the initial crack. Beyond an axial displacement of 5 mm, the auxetic tube loses its integrity and does not contribute to the load carry capability of the hybrid tube anymore. This can be noticed in Point ② of Fig. 11. However, the initial constraint

from the auxetic tube has changed the deformation of the inner conventional tube. The first lobe formed in the conventional tube was an axisymmetric lobe, after that the deformation mode of the conventional tube changed to diamond mode. Point ③ in the Fig. 11 shows the deformed tube with one axisymmetric lobe, one diamond lobe and another diamond lobe in formation. At a displacement of approximately 75 mm (Point ④ in Fig. 11), the inner conventional tube is fully compressed with one axisymmetric lobe and two diamond lobes. The simulated deformation mode matched very well with experimental deformation mode. The simulated tube has one axisymmetric lobe and two diamond lobes (Point ④ in Fig. 11b), similar to what is observed in the experiment. However, the axisymmetric lobe appears at a later stage (i.e. a larger axial displacement). Both the experimental and numerical results show that the failure of the auxetic tube starts near the bottom layer of the outer auxetic tube, which is highlighted in the yellow boxes in Fig. 13.

The initial peak forces (Fig. 12) of the hybrid tube are approximately 59 kN and 65 kN for the experiment and the FEA, respectively. The difference in the peak force is approximately 10%. The experimentally measured and numerically simulated mean forces of the hybrid tube are 27 kN and 25 kN respectively, with a difference less than 8%. The discrepancy in the pattern on the force-displacement curve is because the axisymmetric lobe formed in the inner tube at a later stage of the compression in the numerical simulation, while it formed early in the experiment.

The radial contraction observed in both experiments and FEA is only approximately 0.25 mm, which is the original gap between the inner surface of the auxetic tube and the outer surface of the conventional tube (mentioned in Section 2.1). Due to the strong resistance from the inner conventional tube, there was no further radial contraction in the outer auxetic tube.

5. Discussions

5.1. Effect of auxetic tube

To understand the role of the auxetic tube on the performance of the hybrid tube, numerically simulated force-displacement curves of all three types of tubes are shown in Fig. 14. The curve “Auxetic tube + conventional tube” indicates the summation of force values of auxetic tube and conventional tube. The initial peak forces of the auxetic and the conventional tubes are 5.6 kN and 40 kN. The sum of these two initial peak forces is 45.6 kN. However, the initial peak force of the hybrid tube is 65 kN, which is 43% higher than that of the sum of the auxetic and the conventional tubes. This increase in the initial peak force is solely because of the interaction between the auxetic and the conventional tubes. The mean force of the hybrid tube is 14% higher than that of the sum of the auxetic and the conventional tubes, respectively.

To understand the cause for the change in deformation mode, the interaction force exerted on the conventional tube by the outer auxetic tube is shown in Fig. 15. The interaction force between the tubes spike just after initial failure of the outer auxetic tube. This indicates that the non-failed portion of the auxetic tube exerts a significant force (approximately 2 kN) on the conventional tube, which changed the deformation mode from axisymmetric to diamond mode of the inner conventional tube.

The effect of the auxetic tube on the energy absorption (EA) and specific energy absorption (SEA) is shown in Fig. 16. EA is calculated as the area under the force-displacement curve. SEA is calculated by dividing the EA by the mass of the tube. The EA (Fig. 16a) of the hybrid tube was higher than that of the auxetic tube and conventional tube because hybrid tube consists of both auxetic and conventional tubes. Moreover, the EA of the hybrid tube is also greater than that of the sum of auxetic and conventional tube, which indicates there is interaction between the outer auxetic and inner conventional tube in their hybrid configuration. However, the SEA (Fig. 16b) of the auxetic tube is far lesser than that of the conventional and the hybrid tubes. Moreover, the SEA of the hybrid tube is lesser than that of the conventional

tube. The SEA of the hybrid tube is 38% lesser than that of the conventional tube at the displacement of 50 mm. In hybrid tube, the outer auxetic tube failed very early under the axial compression and did not contribute to the energy absorption after the early failure. Material with higher ductility or higher strength may result in better performance as discussed in the following sections. The SEA of the "auxetic tube + conventional tube" is calculated by dividing energy absorption by the summation of the mass of both the tubes. The SEA of the hybrid tube is found to be slightly higher than the SEA of the "auxetic tube + conventional tube". This indicates that the hybrid tube dissipates more energy through interaction of the outer and inner tubes.

5.2. Effect of conventional tube's wall thickness

The outer auxetic tube in the hybrid tube failed very early under the compression. There are two possible solutions to rectify this issue. Firstly, the failure regions (i.e. portions between two holes) in the auxetic tube is strengthened by increasing material, i.e. by reducing the number of holes in the auxetic tube. Two more numerical simulations were conducted using another two designs of outer tubes – one outer tube with less number of elliptical holes and the other outer tube with the same number of circular holes (instead of elliptical holes in the experiments). The results showed that the auxetic behavior of these two types of tubes vanished. The results are not shown here for the sake of brevity. Secondly, the wall thickness of the inner conventional tube can be reduced so that its resistance to outer auxetic tube also decreases. In this section, the wall thickness of the inner conventional tube was varied to 0.5 mm and 1 mm. The results were compared with the inner conventional tube of 1.5 mm thickness.

Deformation modes of the conventional tubes with wall thickness of 0.5 mm and 1 mm are shown in Fig. 17. A mixed-mode of deformation was observed for the tube with 0.5 mm

wall thickness and axisymmetric mode with eight lobes was observed for the tube with 1 mm wall thickness. Figure 18 shows the deformation of hybrid tubes with inner conventional tube wall thickness of 0.5 mm and 1 mm. The outer auxetic tube failed (highlighted in the yellow box) at a displacement of 4 mm for both the cases. This signifies that the outer auxetic tube is still not strong or ductile enough to withstand the force from the inner tube. The presence of the outer auxetic tube changed the deformation mode of the inner conventional tubes by exerting force on the outer surface of the conventional tube. Force-displacement curves of the conventional tube and the hybrid tube for both the wall thicknesses are shown in Fig. 19. The initial peak forces of the conventional tube of 0.5 mm thickness and the hybrid tube are 12.9 kN and 34.7 kN, respectively. The mean forces of the conventional tube of 0.5 mm thickness and the hybrid tube are 3.8 kN and 9.0 kN, respectively, with an increase of 138% in the mean force for the hybrid tubes. For 1 mm thick conventional tube and the corresponding hybrid tube, the initial peak forces are 26.9 kN and 51.8 kN, respectively; and the mean forces are 12.4 kN and 16.4 kN for conventional tube and hybrid tube respectively.

Figure 20 shows the SEA of the tubes with the inner tube wall thickness of 0.5 mm, 1 mm, and 1.5 mm. The SEA of the hybrid tubes is still less than the conventional tubes for all the wall thicknesses. At a displacement of 50 mm, the SEA of the hybrid tube is 36%, 39%, and 38% lesser than that of the conventional tube of 0.5 mm, 1 mm, and 1.5 mm thicknesses, respectively. As discussed before, the early failure of the outer auxetic tube is the reason for the reduction in SEA. However, the SEA of the hybrid tube was higher than the SEA of the "auxetic tube + conventional tube" for all the cases.

5.3. Fracture locus and failure strain

It should be noted that the failure strains of the elements in the auxetic tube and the hybrid tube are different. When the elements failed, the effective plastic strain was approximately 0.77 for the auxetic tube and 0.40 for the hybrid tube. This variation in failure strain is because of

the stress states (i.e. the stress triaxiality) of the elements at the time when the failure occurred. The stress triaxialities were 0.25 and 0.52 at the time of failure for the elements of the auxetic tube and the hybrid tube, respectively. As shown in Fig. 5, the failure strain is less for higher stress triaxiality when stress triaxiality is less than 0.6. This is the reason for the early failure of the hybrid tube.

To understand the effect of failure strain on the deformation mode and energy absorption, failure strain of the outer auxetic tube in the hybrid tube was varied from 0.5 to 0.7 (without using fracture locus) at an interval of 0.1 in the FE models. The thickness of the inner conventional tube was kept as 0.5 mm. When the magnitude of the failure strain was increased to 0.5, a small change in deformation mode was observed (Fig. 21). When compared with triaxial based failure criteria (Fig. 21a), a kink was formed in the middle of the hybrid tube when the failure strain was increased to 0.5 (Fig. 21b). Further increase in failure strain did not generate any significant effect on the deformation mode. The failure of the outer auxetic tube in the hybrid tube happened at the same location for all failure strains between 0.5 and 0.7, as shown in Fig. 21 (highlighted in yellow boxes). Figure 22 shows the SEA of the hybrid tubes for various failure strains. The SEA increases with the increase in failure strain. This indicates that the material with better ductility is expected to absorb a higher energy without any increase in mass.

5.4. Effect of the yield strength of auxetic tube material

In this section, the performance of the hybrid tube was evaluated by varying yield strength of the material used for the auxetic tube is discussed. The thickness of the inner conventional tube is kept at 0.5 mm. The yield strength of the auxetic tube was increased to 300 MPa, 400 MPa, and 500 MPa, respectively. Apart from yield strength, all the remaining parameters, such as, density, Young's modulus, tangent modulus, and Poisson's ratio were

unchanged. The failure criterion was not employed for the auxetic tube. The deformation pattern of the auxetic tube followed the same pattern as the one shown in Figs. 8. This implies that the deformation mode of the auxetic tube is unaffected by the tube material's yield strength.

The deformation mode (Fig. 23) and force-displacement curves (Fig. 24) were examined in detail. As the yield strength increases, all the hybrid tubes exhibited auxetic behaviour. This can be noticed at the displacement of 10 mm for all three cases with yield strengths of 300 MPa, 400 MPa, and 500 MPa, respectively. Upon further compression, at the displacements of 25 mm and 50 mm, localized deformation was observed. Force-displacement curves in Fig. 24 shows that initial peak force increases as yield strength of the auxetic tube increases. After the initial peak, the force fluctuates, which is when the hybrid tube exhibited auxetic behaviour. Once the localized deformation starts, the force starts decreasing.

The SEA of the tubes is shown in Fig. 25. In terms of SEA, the hybrid tube performed better than the auxetic tube, the conventional tube, and the "auxetic tube + conventional tube" for all the three cases studied. Moreover, as the yield strength of the auxetic tube increases, the SEA of the hybrid tube is significantly higher than that of the conventional tube. For the auxetic tube's material with the yield strength of 500 MPa, the SEA of the hybrid tube is 179% higher than that of the conventional tube. The improvement in SEA of hybrid tube is attributed to the stronger outer tube. As the strength of the outer tube increases, the deformation of inner tube had to comply with the deformation of the outer tube, resulting in larger crushing force and greater energy dissipation.

6. Conclusions

In this study, the design and mechanical response of a novel hybrid tube was explored experimentally and numerically. The architecture of the hybrid tube comprised a conventional tube as the inner tube and an auxetic tube as the outer tube. Mutually orthogonal elliptical holes

were cut on a conventional tube to obtain an auxetic tube. The auxetic tubes were fabricated from aluminum alloy 6060 T5 using conventional machining technology. The auxetic, the conventional, and the hybrid tubes were subjected to axial quasi-static compression. Three-dimensional digital image correlation technique was employed to capture the displacement fields on the periphery of the tubes. Three different FE models were also developed for all the three types of tubes using ANSYS/LS-DYNA and FE results were corroborated by the experimental results.

Deformation mode observed in the FEA matched well with the experimental results of conventional tubes. The numerically simulated results of the auxetic tube and hybrid tube matched reasonably well with the experimental results in terms of deformation mode and the general trend of the force-displacement curve. A discrepancy in the experimentally measured and numerically simulated peak forces of auxetic tube was observed.

Both experimental and numerical results showed that the conventional tubes exhibited six axisymmetric lobes with a mean force of 21.5 kN. Auxetic tube contracted through the collapse of elliptical holes and failed at an axial displacement of approximately 45 mm. Post-processed DIC images revealed that the radius of the auxetic tube shrank by up to approximately 5 mm (20% reduction in radius). The auxetic tube exhibited an initial peak force of 5.6 kN. For the hybrid tube, the outer auxetic tube contracted and exerted transverse force on the inner conventional tube, which changed its deformation mode. The interaction force was approximately 3% of the axial force. Outer auxetic tube failed at a relatively small displacement of approximately 2.8 mm. The initial peak force and the mean force were higher for the hybrid tube when compared with those of the conventional and auxetic tubes. The specific energy absorption of the hybrid tube was lesser than that of the conventional tube. The outer auxetic tube failed at an early stage of the compression and did not contribute much to the load carrying

capacity of the hybrid tube. However, its mass is still being accounted for SEA calculation, which reduced the SEA of the hybrid tube.

Because of the greater stress triaxiality, the failure strain of the hybrid tube was less than that of the auxetic tube. Increasing the failure strain or yield strength resulted in better load carrying capacity and SEA of the hybrid tube, which indicates that by employing an outer auxetic tube made from ductile and high yield strength material will enhance both the load carry capacity and energy absorption of hybrid tubes.

Acknowledgements

The authors would like to acknowledge, with thanks, Mr. Kevin Nievaart for his guidance in three-dimensional digital image correlation setup and post-processing. The authors would also like to acknowledge and appreciate the financial supports from Ministry of Education (MoE), India through SPARC scheme (SPARC/2018-2019/P988/SL).

References

[1] T.A. Schaedler, W.B. Carter, Architected Cellular Materials, Annu. Rev. Mater. Res. 46 (2016) 187–210. https://doi.org/10.1146/annurev-matsci-070115-031624.

[2] S. Kumar, J. Ubaid, R. Abishera, A. Schiffer, V.S. Deshpande, Tunable Energy Absorption Characteristics of Architected Honeycombs Enabled via Additive Manufacturing, ACS Appl. Mater. Interfaces. 11 (2019) 42549–42560. https://doi.org/10.1021/acsami.9b12880.

[3] J.N. Grima, K.E. Evans, Auxetic behavior from rotating squares, J. Mater. Sci. Lett. 19 (2000) 1563–1565. https://doi.org/10.1023/A:1006781224002.

[4] J.N. Grima, R. Gatt, A. Alderson, K.E. Evans, On the potential of connected stars as auxetic systems, Mol. Simul. 31 (2005) 925–935.

https://doi.org/10.1080/08927020500401139.

[5] J.N. Grima, R. Gatt, Perforated sheets exhibiting negative Poisson's ratios, Adv. Eng. Mater. 12 (2010) 460–464. https://doi.org/10.1002/adem.201000005.

[6] N. Gaspar, X.J. Ren, C.W. Smith, J.N. Grima, K.E. Evans, Novel honeycombs with auxetic behaviour, Acta Mater. 53 (2005) 2439–2445. https://doi.org/10.1016/j.actamat.2005.02.006.

[7] K. Bertoldi, P.M. Reis, S. Willshaw, T. Mullin, Negative poisson's ratio behavior induced by an elastic instability, Adv. Mater. 22 (2010) 361–366. https://doi.org/10.1002/adma.200901956.

[8] J. Shen, S. Zhou, X. Huang, Y.M. Xie, Simple cubic three-dimensional auxetic metamaterials, Phys. Status Solidi Basic Res. 251 (2014) 1515–1522. https://doi.org/10.1002/pssb.201451304.

[9] D. Li, J. Ma, L. Dong, R.S. Lakes, Stiff square structure with a negative Poisson's ratio, Mater. Lett. 188 (2017) 149–151. https://doi.org/10.1016/j.matlet.2016.11.036.

[10] X. Ren, R. Das, P. Tran, T.D. Ngo, Y.M. Xie, Auxetic metamaterials and structures: a review, Smart Mater. Struct. 27 (2018) 023001. https://doi.org/10.1088/1361-665X/aaa61c.

[11] M.N. Ali, J.J.C. Busfield, I.U. Rehman, Auxetic oesophageal stents: Structure and mechanical properties, J. Mater. Sci. Mater. Med. 25 (2014) 527–553. https://doi.org/10.1007/s10856-013-5067-2.

[12] X. Ren, J. Shen, P. Tran, T.D. Ngo, Y.M. Xie, Auxetic nail: Design and experimental study, Compos. Struct. 184 (2018) 288–298. https://doi.org/10.1016/j.compstruct.2017.10.013.

[13] K.R.F. Andrews, G.L. England, E. Ghani, Classification of the axial collapse of cylindrical tubes under quasi-static loading, Int. J. Mech. Sci. 25 (1983) 687–696.

https://doi.org/10.1016/0020-7403(83)90076-0.

[14] N. Baaskaran, K. Ponappa, S. Shankar, Quasi-static crushing and energy absorption characteristics of thin-walled cylinders with geometric discontinuities of various aspect ratios, Lat. Am. J. Solids Struct. 14 (2017) 1767–1787. https://doi.org/10.1590/1679-78253866.

[15] S.B. Bodlani, S. Chung Kim Yuen, G.N. Nurick, The energy absorption characteristics of square mild steel tubes with multiple induced circular hole discontinuities-part I: Experiments, J. Appl. Mech. Trans. ASME. 76 (2009) 1–11. https://doi.org/10.1115/1.3114971.

[16] R.D. Hussein, D. Ruan, G. Lu, S. Guillow, J.W. Yoon, Crushing response of square aluminium tubes filled with polyurethane foam and aluminium honeycomb, Thin-Walled Struct. 110 (2017) 140–154. https://doi.org/10.1016/j.tws.2016.10.023.

[17] A. Ghamarian, H.R. Zarei, M.T. Abadi, Experimental and numerical crashworthiness investigation of empty and foam-filled end-capped conical tubes, Thin-Walled Struct. 49 (2011) 1312–1319. https://doi.org/10.1016/j.tws.2011.03.005.

[18] Q. Liu, Z. Mo, Y. Wu, J. Ma, G.C. Pong Tsui, D. Hui, Crush response of CFRP square tube filled with aluminum honeycomb, Compos. Part B Eng. 98 (2016) 406–414. https://doi.org/10.1016/j.compositesb.2016.05.048.

[19] Y. Zhang, L. Yan, W. Zhang, P. Su, B. Han, S. Guo, Metallic tube-reinforced aluminum honeycombs: Compressive and bending performances, Compos. Part B Eng. 171 (2019) 192–203. https://doi.org/10.1016/j.compositesb.2019.04.044.

[20] S. Mohsenizadeh, R. Alipour, M. Shokri Rad, A. Farokhi Nejad, Z. Ahmad, Crashworthiness assessment of auxetic foam-filled tube under quasi-static axial loading, Mater. Des. 88 (2015) 258–268. https://doi.org/10.1016/j.matdes.2015.08.152.

[21] S. Hou, T. Liu, Z. Zhang, X. Han, Q. Li, How does negative Poisson's ratio of foam

filler affect crashworthiness?, Mater. Des. 82 (2015) 247–259. https://doi.org/10.1016/j.matdes.2015.05.050.

[22] R.D. Hussein, D. Ruan, G. Lu, R. Thomson, An energy dissipating mechanism for crushing square aluminium/CFRP tubes, Compos. Struct. 183 (2018) 643–653. https://doi.org/10.1016/j.compstruct.2017.08.033.

[23] K.C. Shin, J.J. Lee, K.H. Kim, M.C. Song, J.S. Huh, Axial crush and bending collapse of an aluminum/GFRP hybrid square tube and its energy absorption capability, Compos. Struct. 57 (2002) 279–287. https://doi.org/10.1016/S0263-8223(02)00094-6.

[24] S. Sharifi, M. Shakeri, H.E. Fakhari, M. Bodaghi, Experimental investigation of bitubal circular energy absorbers under quasi-static axial load, Thin-Walled Struct. 89 (2015) 42–53. https://doi.org/10.1016/j.tws.2014.12.008.

[25] C. Reuter, T. Tröster, Crashworthiness and numerical simulation of hybrid aluminium-CFRP tubes under axial impact, Thin-Walled Struct. 117 (2017) 1–9. https://doi.org/10.1016/j.tws.2017.03.034.

[26] G. Sun, Z. Wang, J. Hong, K. Song, Q. Li, Experimental investigation of the quasi-static axial crushing behavior of filament-wound CFRP and aluminum/CFRP hybrid tubes, Compos. Struct. 194 (2018) 208–225. https://doi.org/10.1016/j.compstruct.2018.02.005.

[27] G. Zhu, G. Sun, Q. Liu, G. Li, Q. Li, On crushing characteristics of different configurations of metal-composites hybrid tubes, Compos. Struct. 175 (2017) 58–69. https://doi.org/10.1016/j.compstruct.2017.04.072.

[28] Z. Wang, X. Jin, Q. Li, G. Sun, On crashworthiness design of hybrid metal-composite structures, Int. J. Mech. Sci. 171 (2020) 105380. https://doi.org/10.1016/j.ijmecsci.2019.105380.

[29] W. Lee, Y. Jeong, J. Yoo, H. Huh, S.J. Park, S.H. Park, J. Yoon, Effect of auxetic

structures on crash behavior of cylindrical tube, Compos. Struct. 208 (2019) 836–846. https://doi.org/10.1016/j.compstruct.2018.10.068.

[30] N. Karnessis, G. Burriesci, Uniaxial and buckling mechanical response of auxetic cellular tubes, Smart Mater. Struct. 22 (2013) 084008. https://doi.org/10.1088/0964-1726/22/8/084008.

[31] X. Ren, J. Shen, A. Ghaedizadeh, H. Tian, Y.M. Xie, A simple auxetic tubular structure with tuneable mechanical properties, Smart Mater. Struct. 25 (2016) 065012. https://doi.org/10.1088/0964-1726/25/6/065012.

[32] X.Y. Zhang, X.Y. Wang, X. Ren, Y.M. Xie, Y. Wu, Y.Y. Zhou, S.L. Wang, C.Z. Han, A novel type of tubular structure with auxeticity both in radial direction and wall thickness, Thin-Walled Struct. 163 (2021) 107758. https://doi.org/10.1016/j.tws.2021.107758.

[33] S.K. Bhullar, J. Ko, Y. Cho, M.B.G. Jun, Fabrication and Characterization of Nonwoven Auxetic Polymer Stent, Polym. - Plast. Technol. Eng. 54 (2015) 1553–1559. https://doi.org/10.1080/03602559.2014.986812.

[34] D.T. Farrell, C. McGinn, G.J. Bennett, Extension twist deformation response of an auxetic cylindrical structure inspired by deformed cell ligaments, Compos. Struct. 238 (2020) 111901. https://doi.org/10.1016/j.compstruct.2020.111901.

[35] C. Luo, C.Z. Han, X.Y. Zhang, X.G. Zhang, X. Ren, Y.M. Xie, Design, manufacturing and applications of auxetic tubular structures: A review, Thin-Walled Struct. 163 (2021). https://doi.org/10.1016/j.tws.2021.107682.

[36] S. Jurendic, R. Burrows, D. Anderson, Damage and Failure Model Characterization for High Strength AA6000 Automotive Aluminium Alloys, 15th Int. LS-DYNA® Users Conf. (2018) 1–8.

Figures:

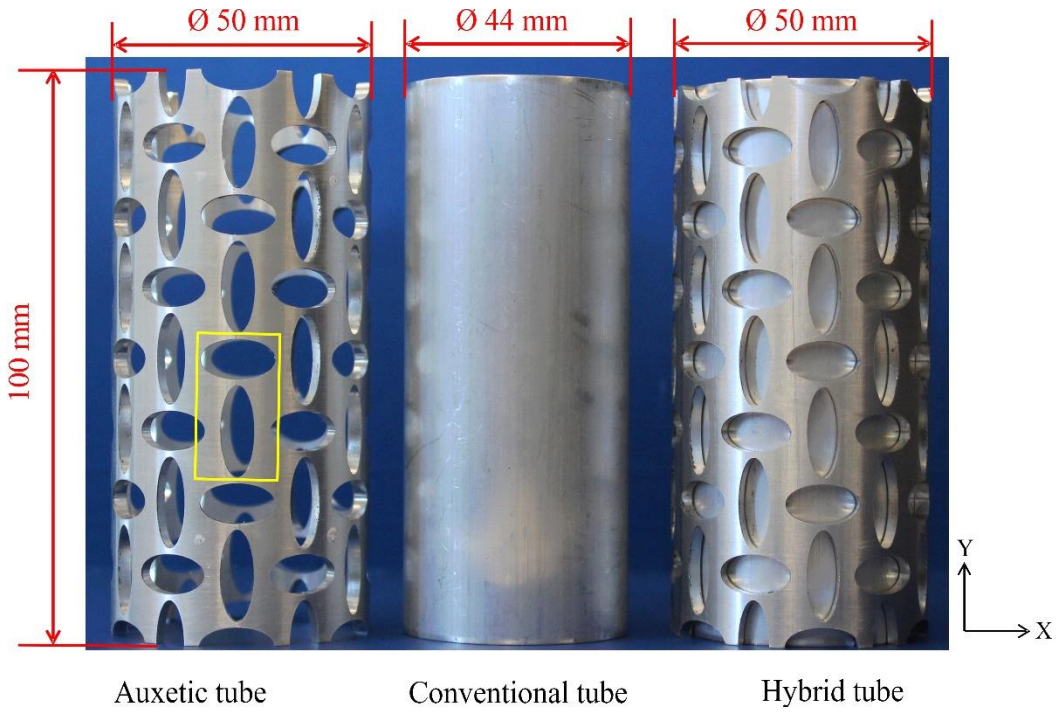

Figure 1. A photograph of the fabricated tubes (a pair of mutually orthogonal elliptical holes are shown in the yellow rectangular box).

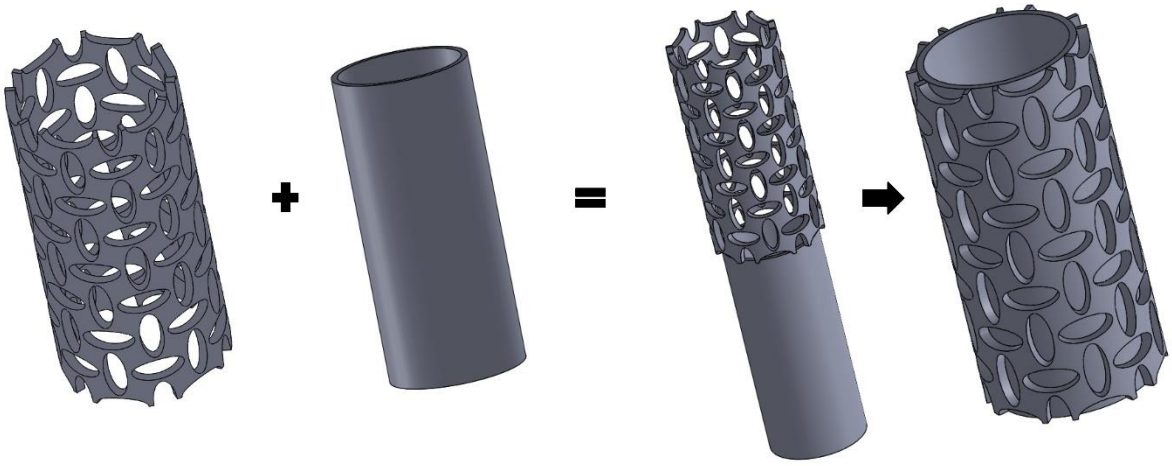

Figure 2. Illustration of a hybrid tube concept.

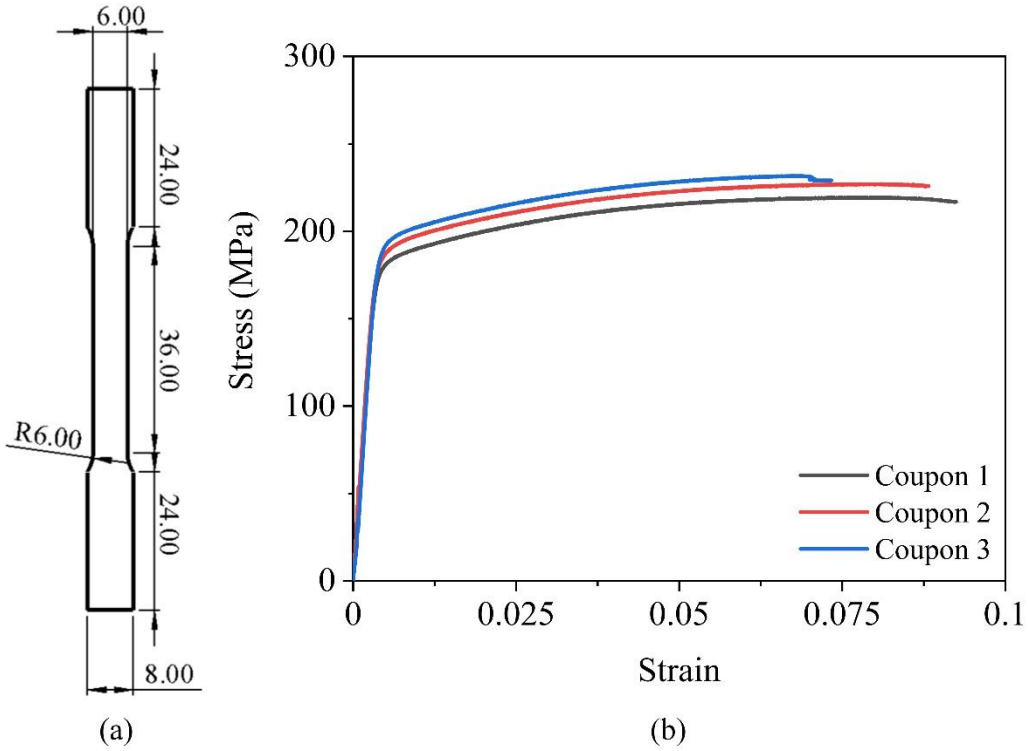

Figure 3. (a) Dimensions (in mm) of the tensile specimens cut from the tube of 50 mm outer diameter; (b) stress-strain curves obtained from the tensile tests of the tube's parent material.

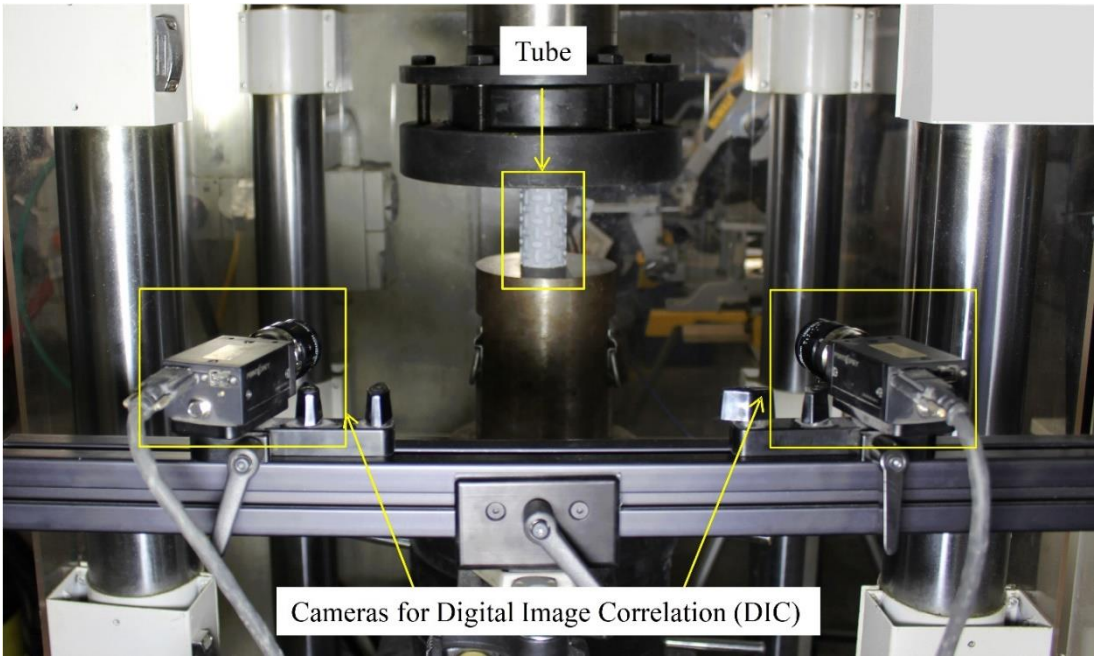

Figure 4. Compressive test setup.

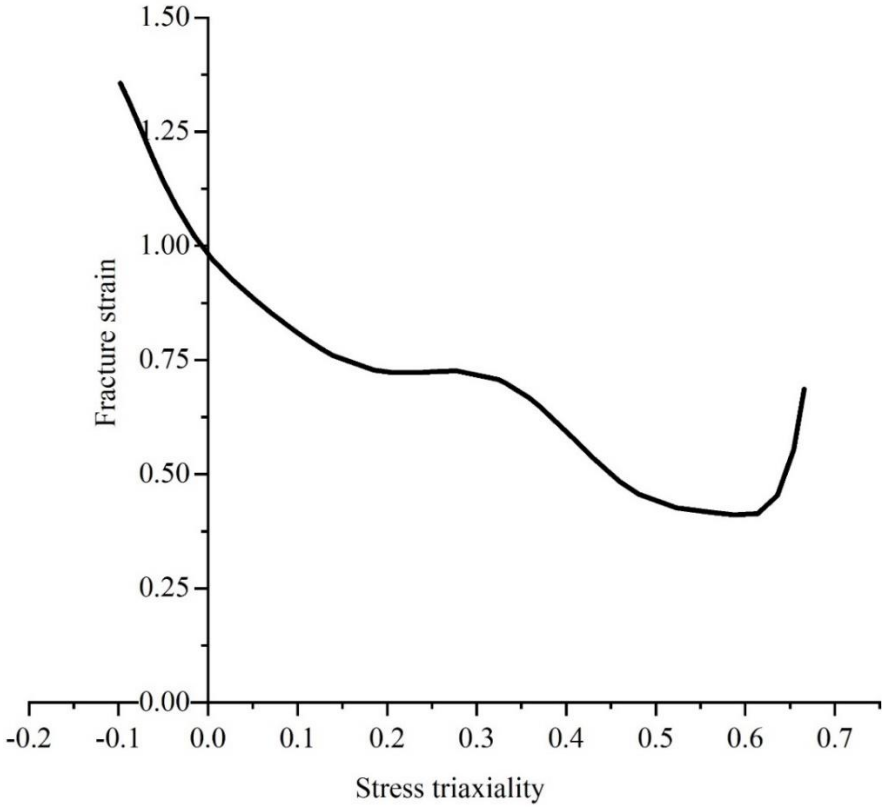

Figure 5. Failure strain *vs.* stress triaxiality curve from the literature [36].

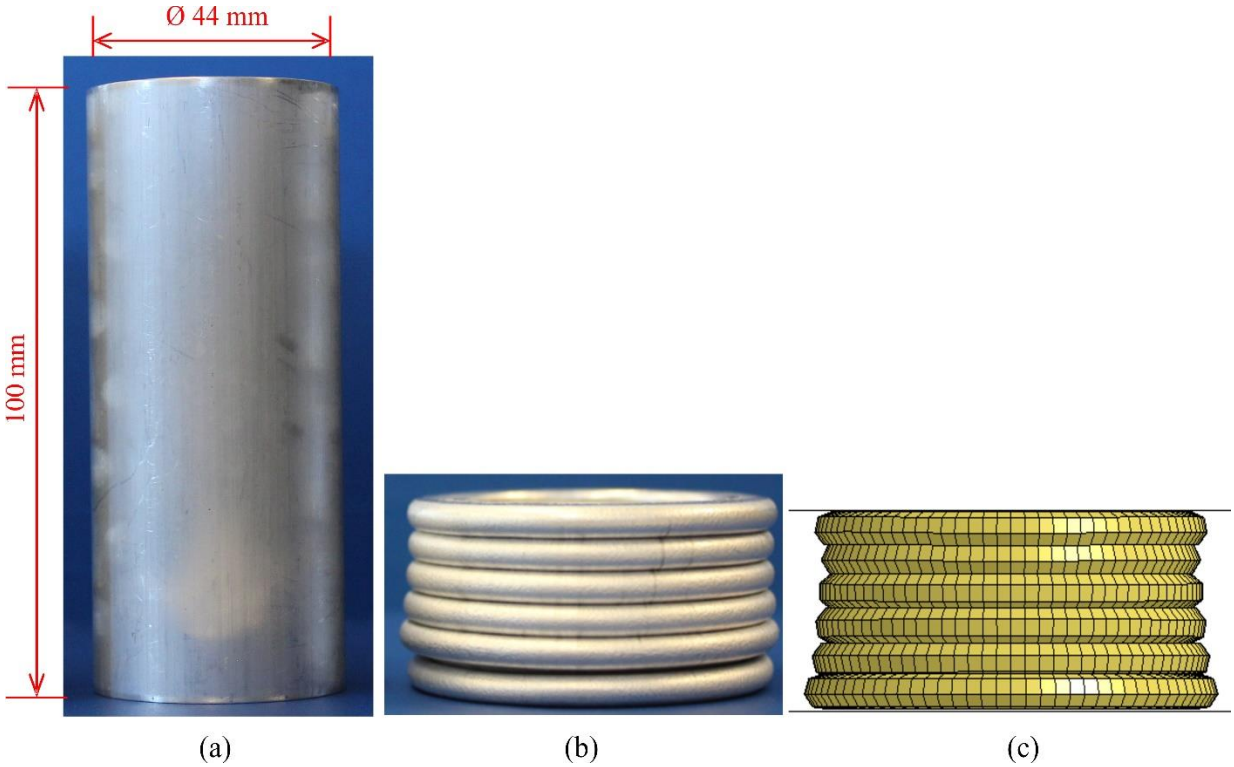

Figure 6. (a) Undeformed conventional tube; (b) deformation modes of the conventional tubes obtained from the experiments; and (c) deformation modes of the conventional tubes obtained the numerical simulation.

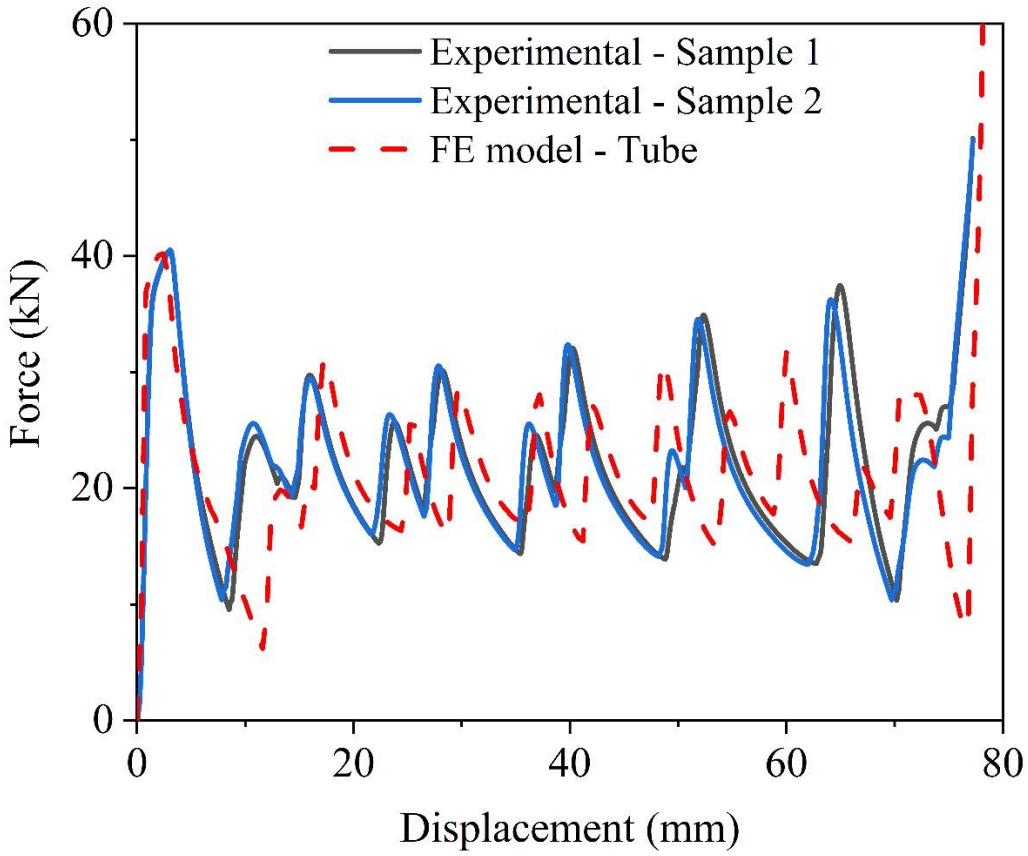

Figure 7. Experimentally measured and numerically simulated force-displacement curves of the conventional tube (D = 44 mm, H = 100 mm, and t = 1.5mm) under axial compression.

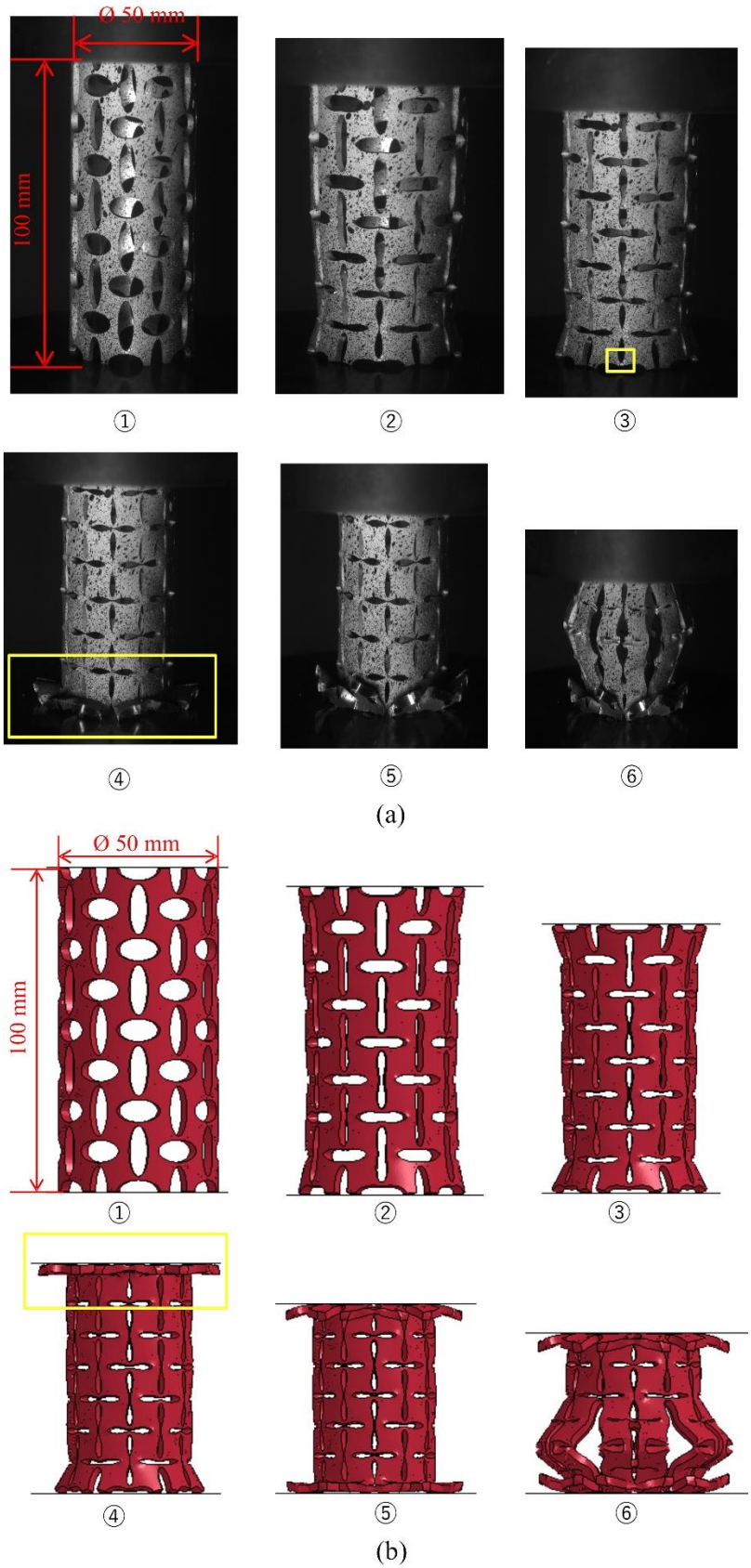

Figure 8. Experimental and numerically simulated deformation mode of auxetic tubes at different stages of axial compression.

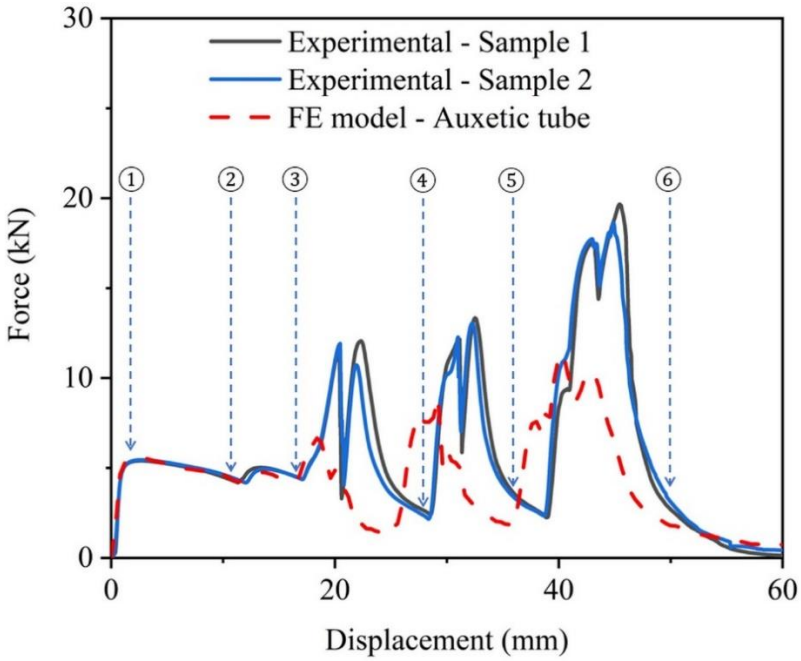

Figure 9. Experimentally measured and numerically simulated force-displacement curves of the auxetic tubes under axial compression.

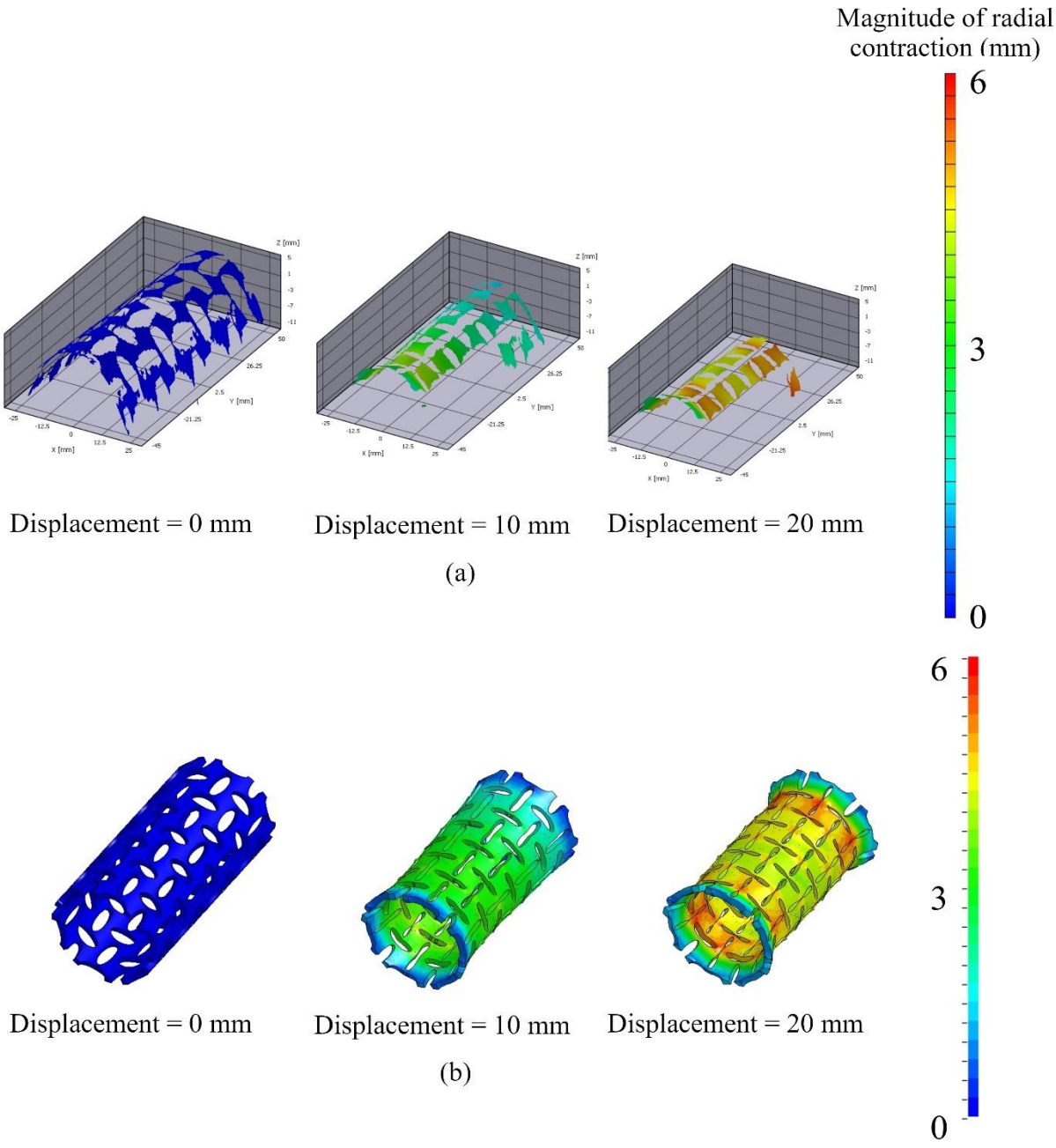

Figure 10. Magnitude of the radial contraction of the auxetic tube (D = 50 mm, H = 100 mm, and t = 3 mm) under axial compression: (a) experimental measurements (Digital Image Correlation); (b) numerical simulation. The displacement values indicated under each image is in the axial direction in mm.

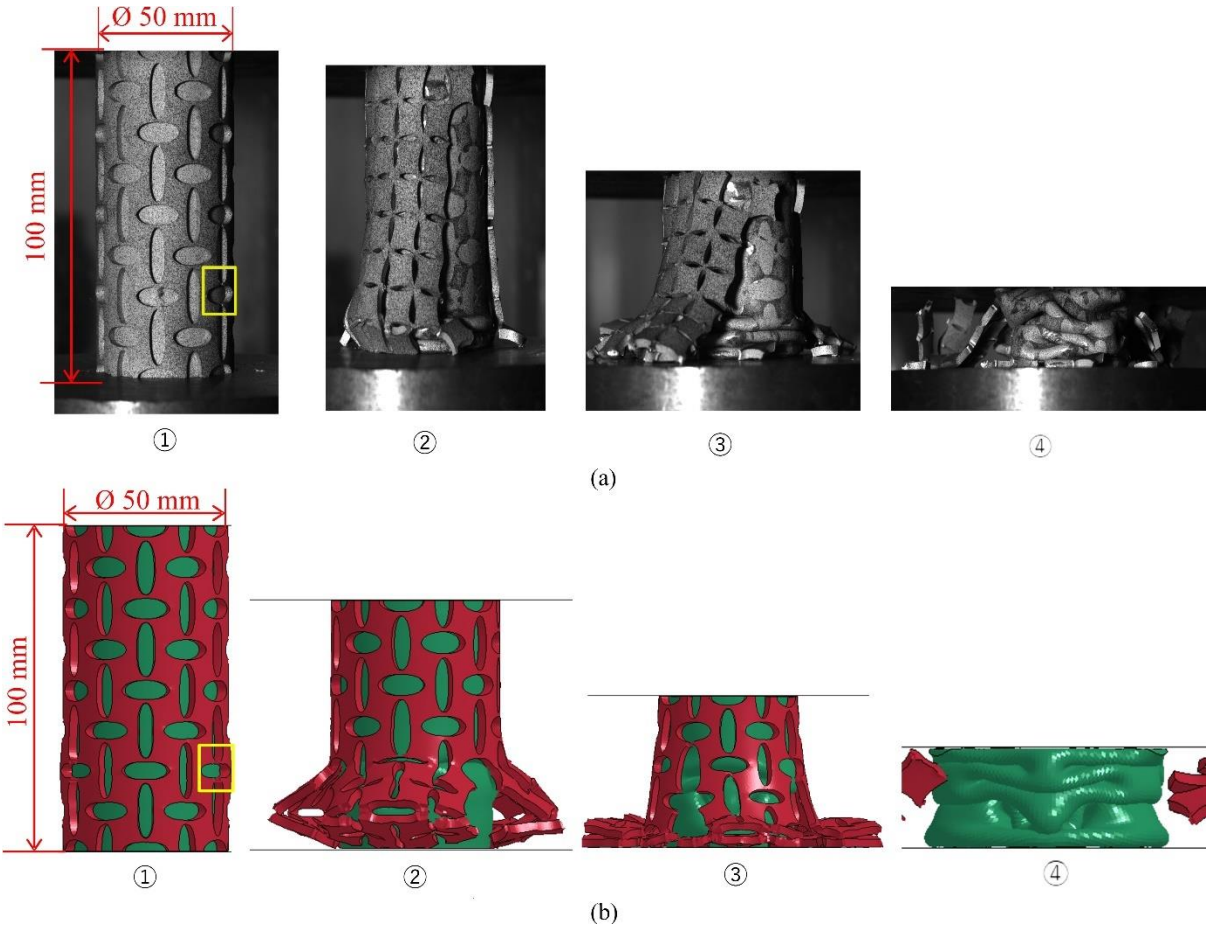

Figure 11. Experimental and numerically simulated deformation mode of hybrid tubes at different stages of axial compression.

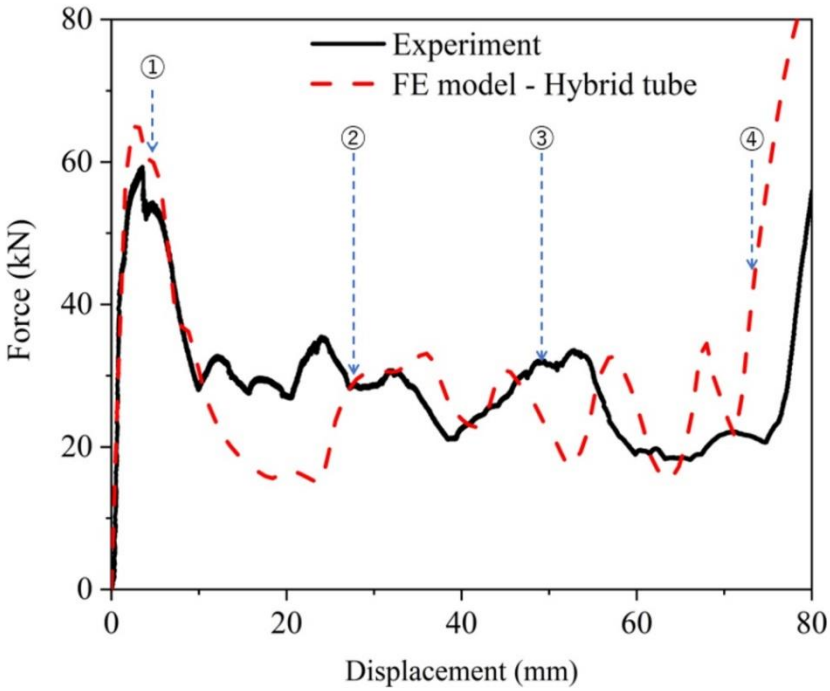

Figure 12. Experimentally measured and numerically simulated force-displacement curves of the hybrid tube under axial compression.

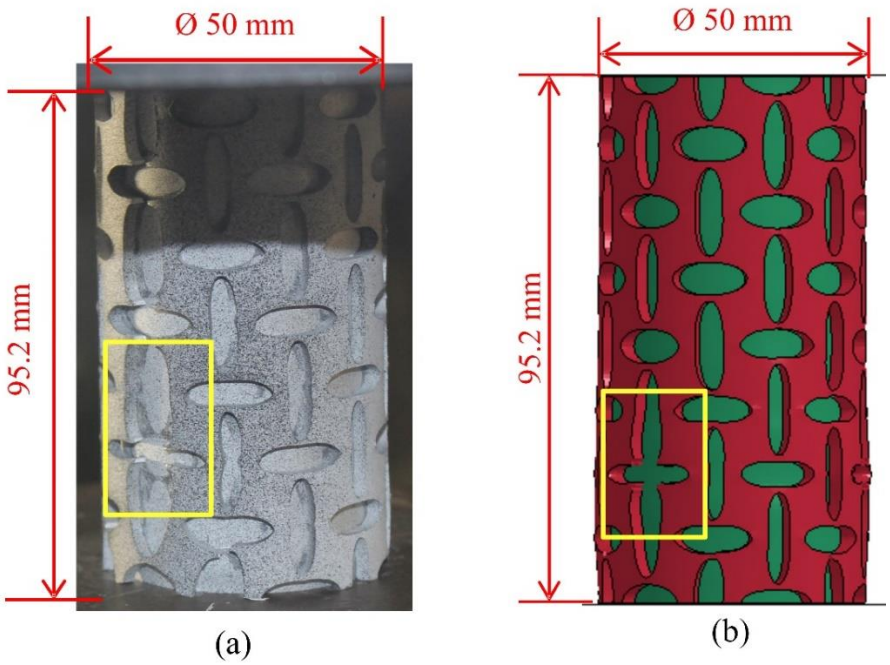

Figure 13. Failure of the hybrid tube observed in (a) the experiment; (b) the FE model (the failure is shown in yellow rectangular boxes).

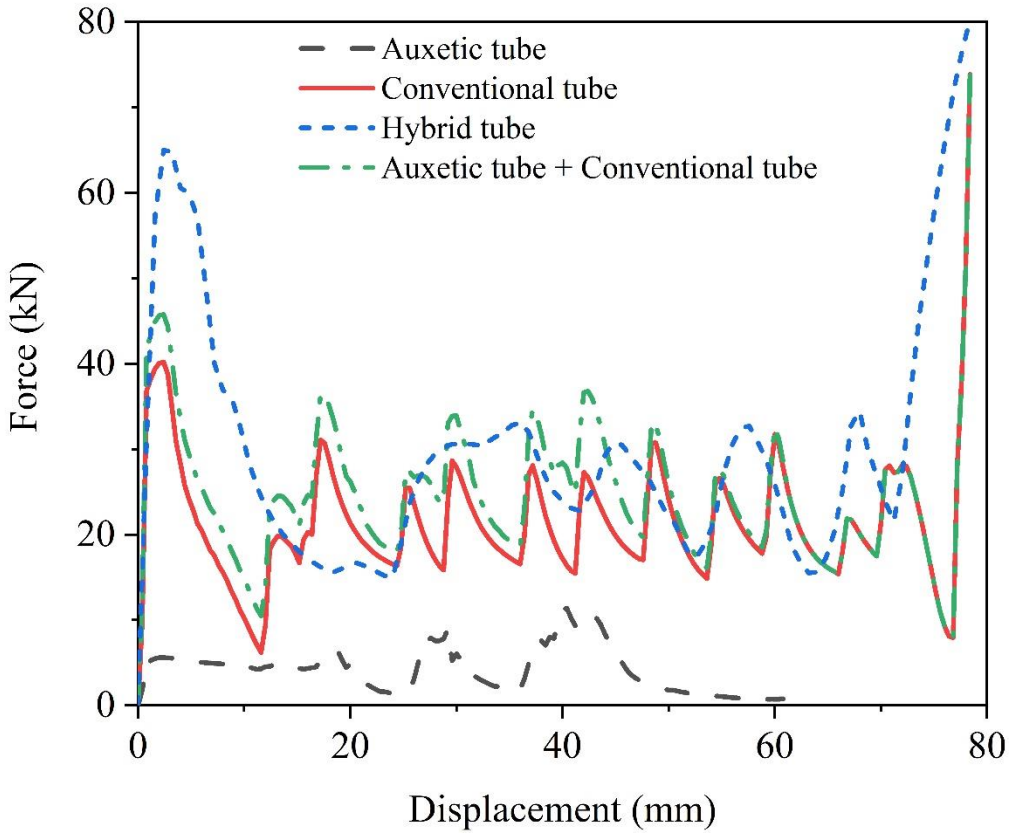

Figure 14. Numerically simulated force-displacement curves of the tubes.

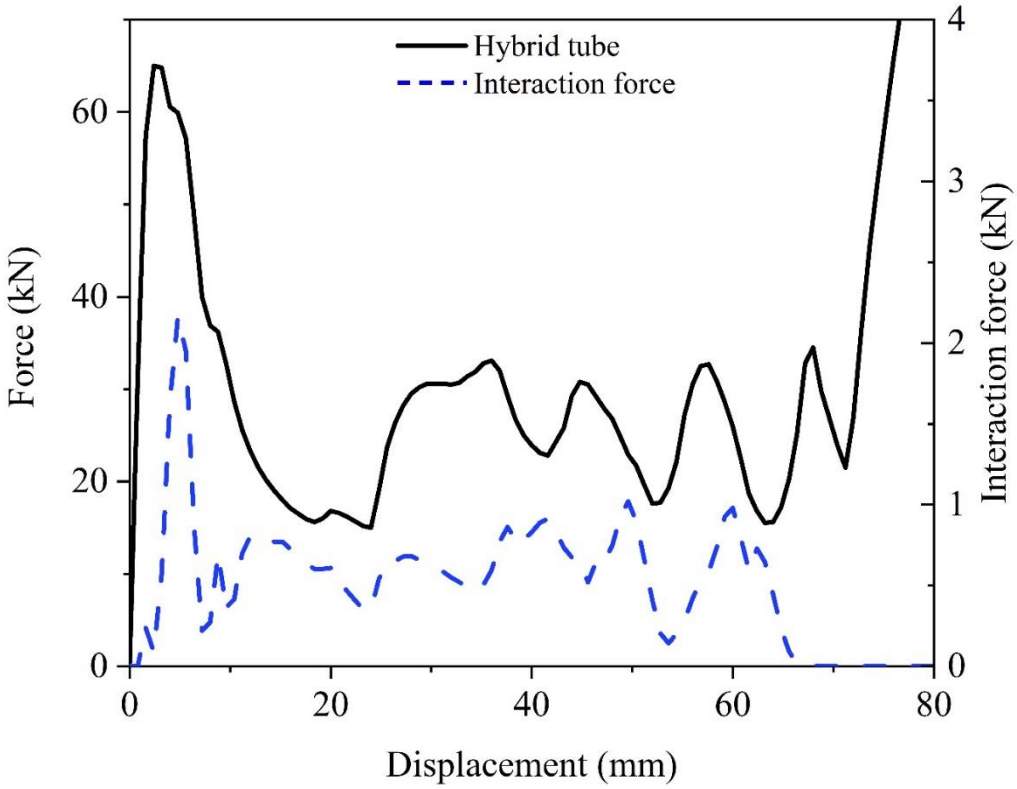

Figure 15. Numerically simulated axial crushing force and interaction force between the inner conventional tube and outer auxetic tube.

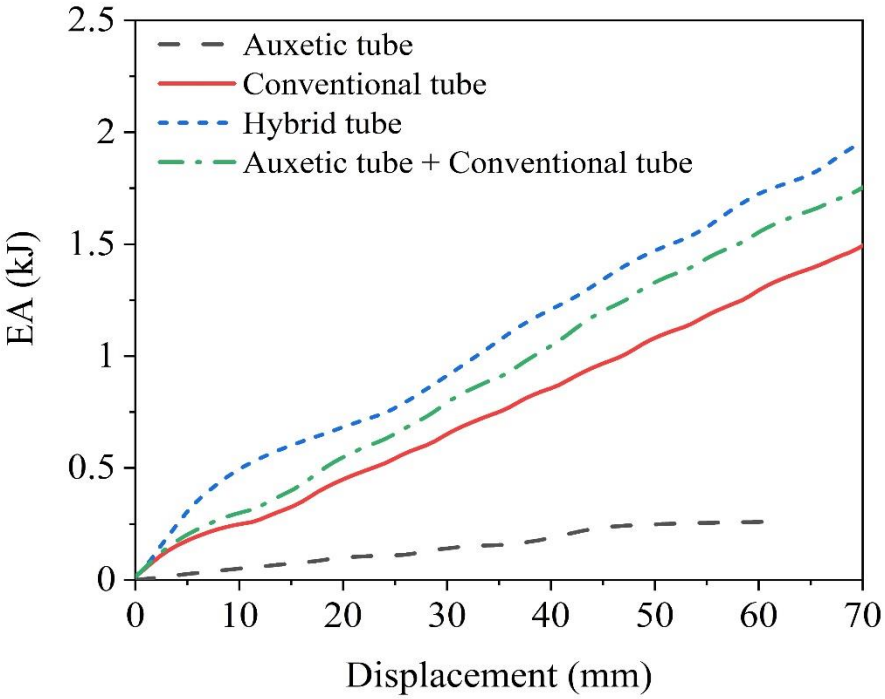

(a)

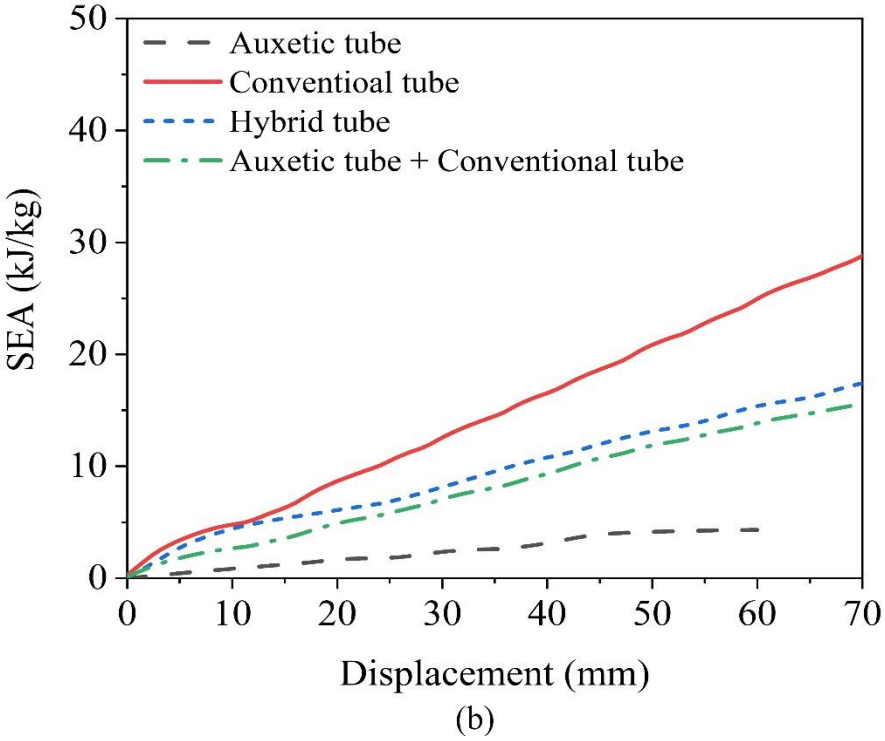

(b)

Figure 16. Numerically simulated: (a) energy absorption; (b) specific energy absorption of the tubes.

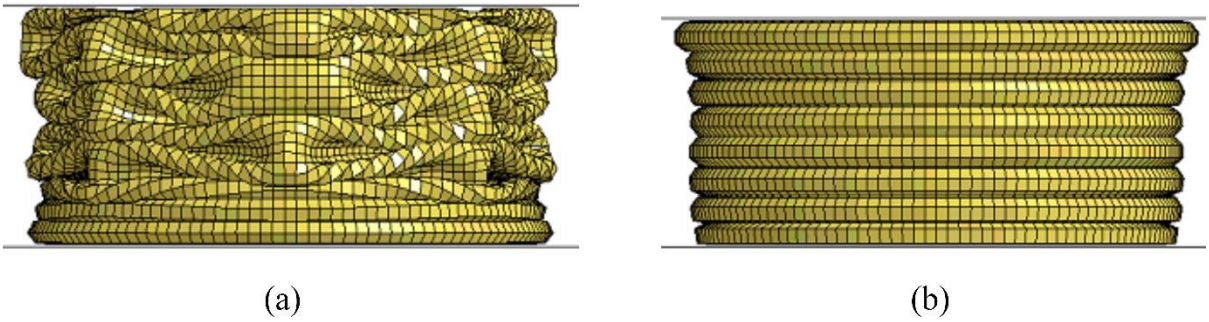

(a) (b)

Figure 17. Numerically simulated deformation modes of conventional tubes (D = 44 mm and H = 100 mm) with different wall thicknesses: (a) 0.5 mm; and (b) 1 mm.

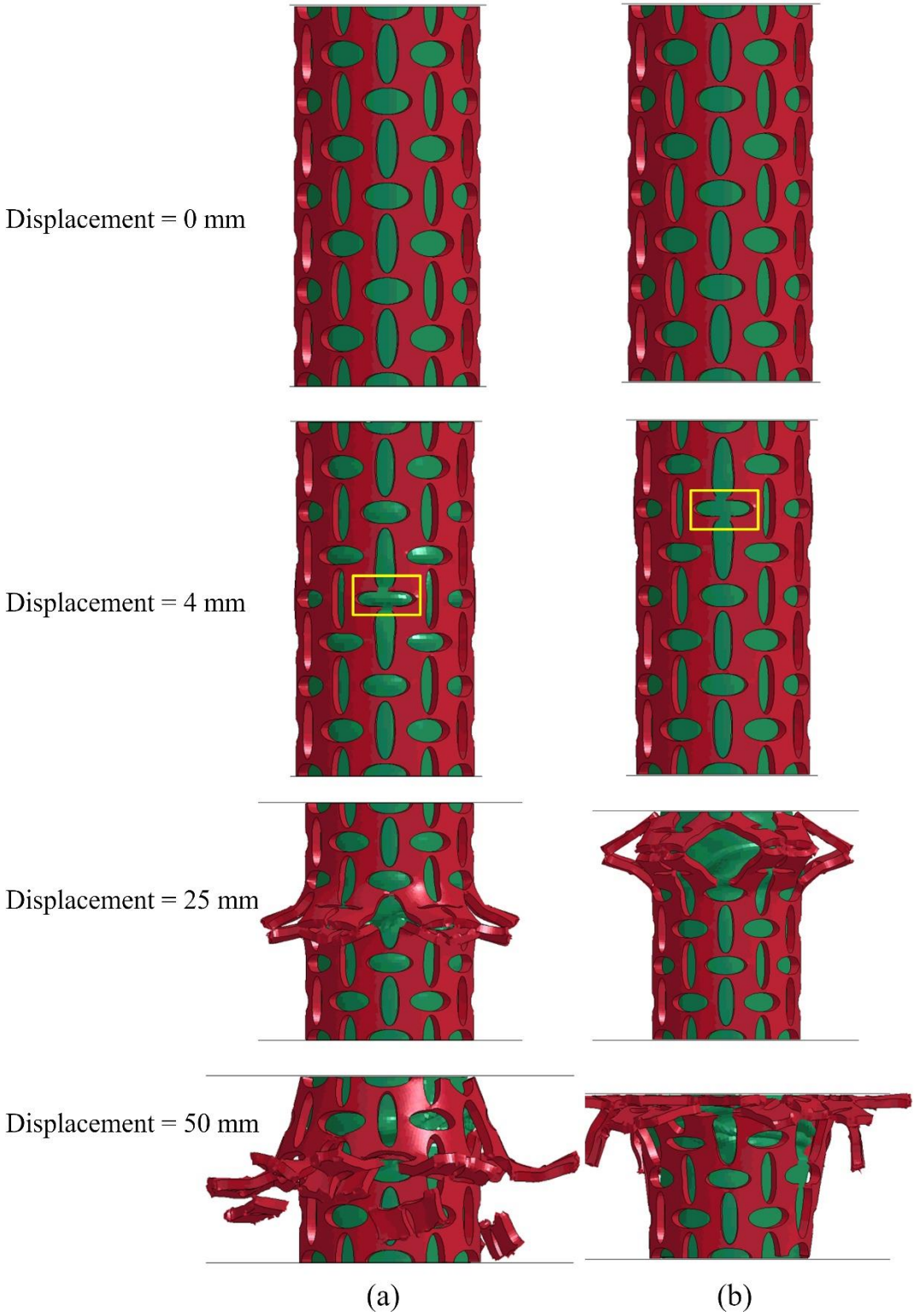

Figure 18. Numerically simulated deformation of hybrid tubes (D = 50 mm and H = 100 mm) at different displacements: (a) inner tube wall thickness is 0.5 mm; and (b) inner tube wall thickness is 1 mm.

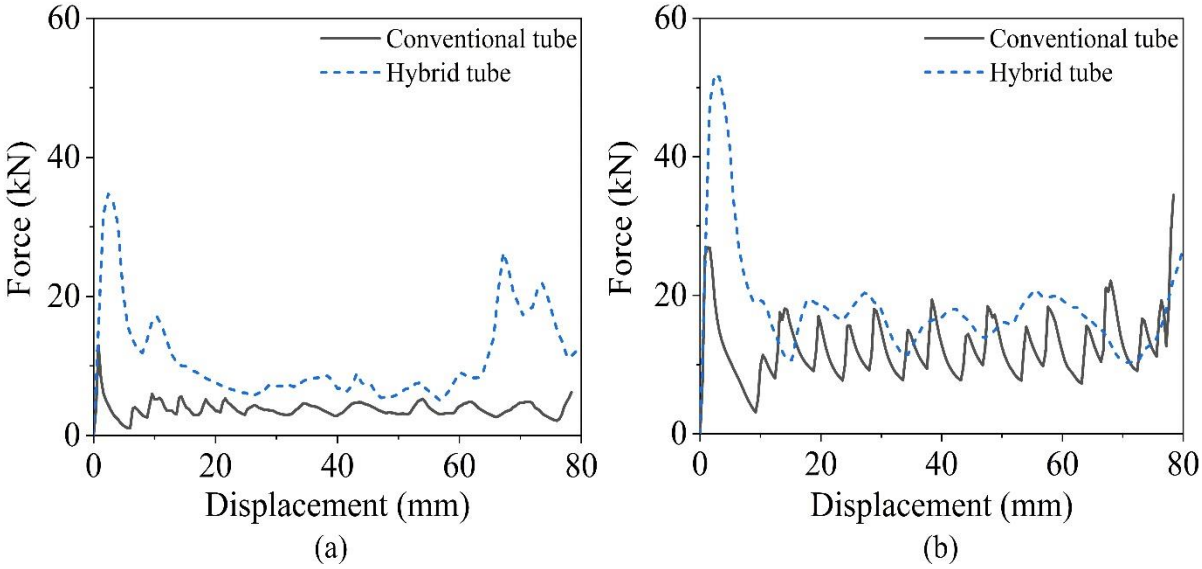

Figure 19. Numerically simulated force-displacement curves of the conventional tubes and hybrid tubes: (a) conventional tube's wall thickness is 0.5 mm; and (b) conventional tube's wall thickness is 1 mm.

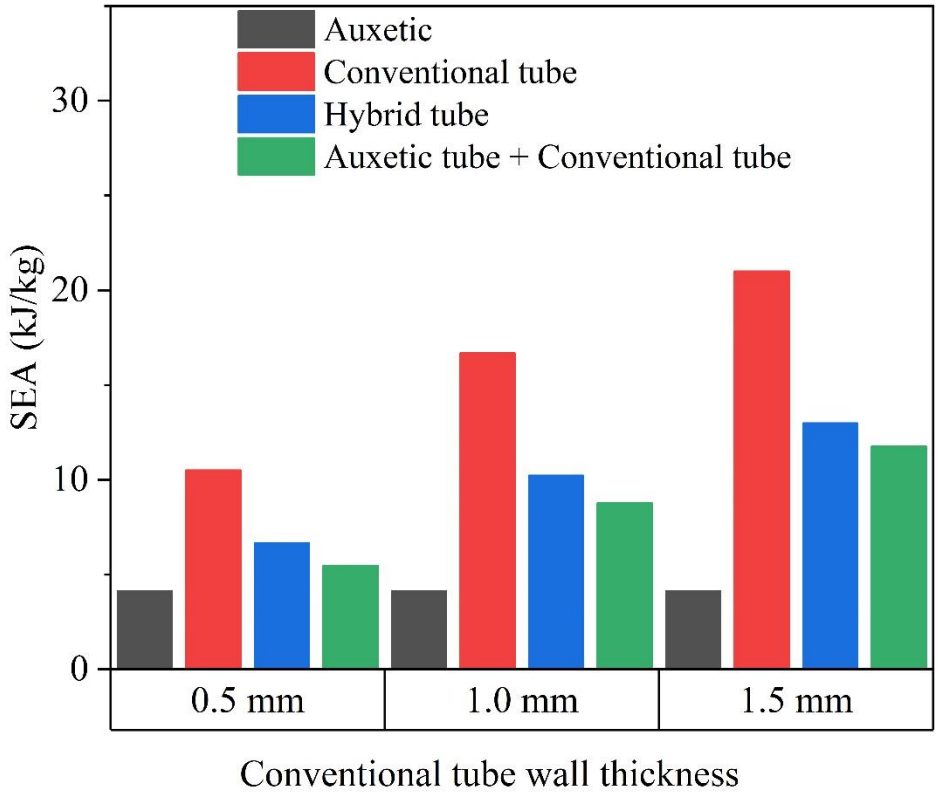

Figure 20. Numerically simulated specific energy absorption of the tubes with different wall thicknesses of the inner conventional tube.

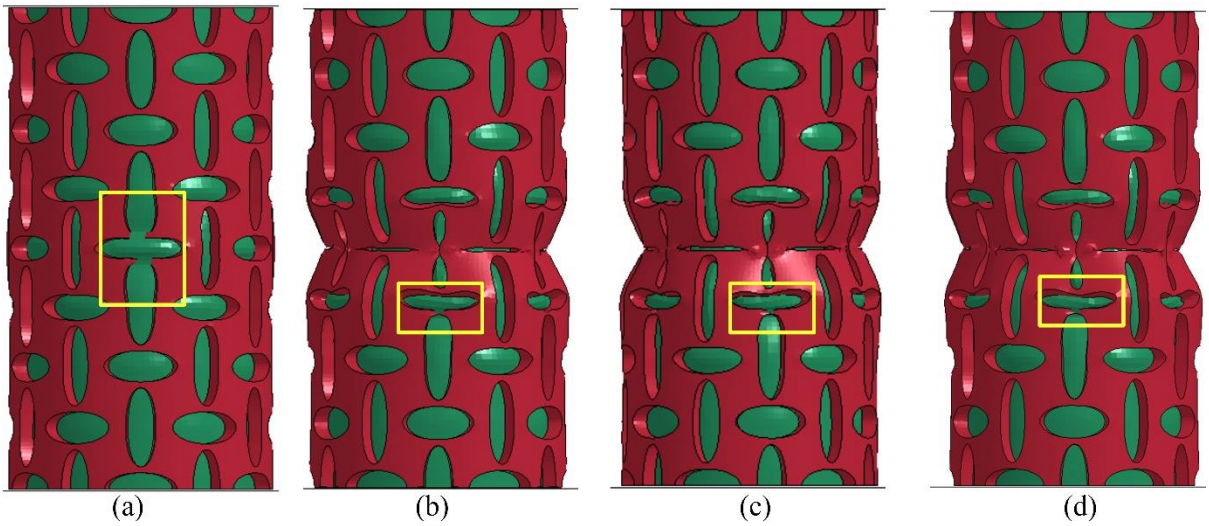

Figure 21. Numerically simulated fracture location in the auxetic tube of the hybrid tube when using a failure strain of: (a) 0.4 (triaxiality locus); (b) 0.5; (c) 0.6; and (d) 0.7.

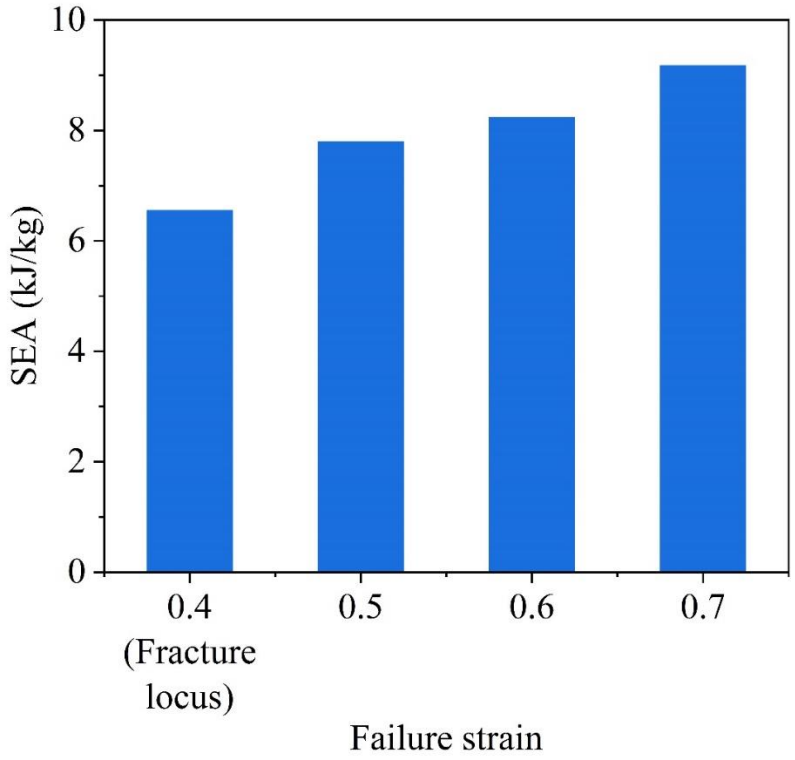

Figure 22. Numerically simulated specific energy absorption of the hybrid tube with different failure strains for the auxetic tube.

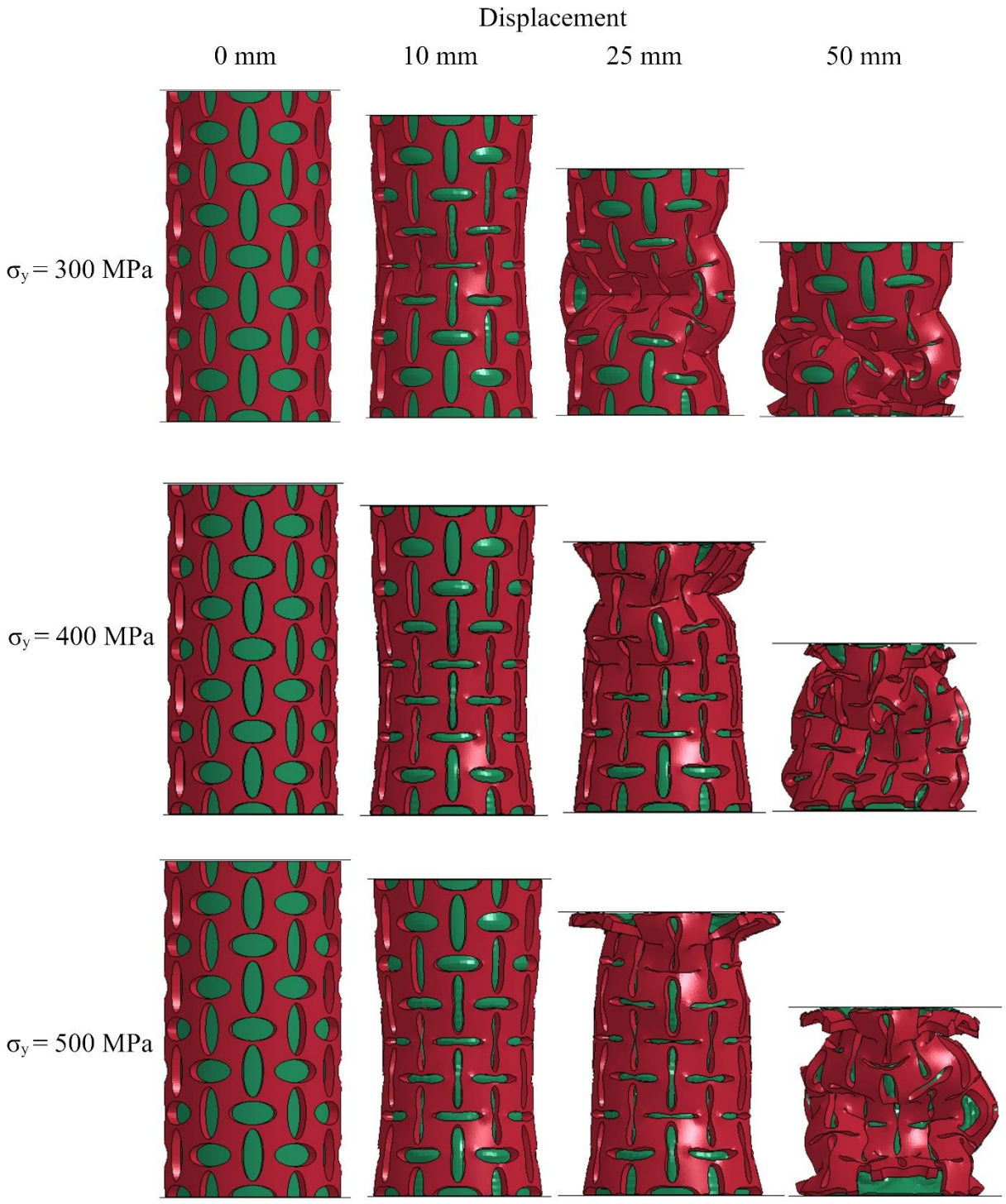

Figure 23. Numerically simulated deformation modes of hybrid tube with different yield strengths of the auxetic tube material.

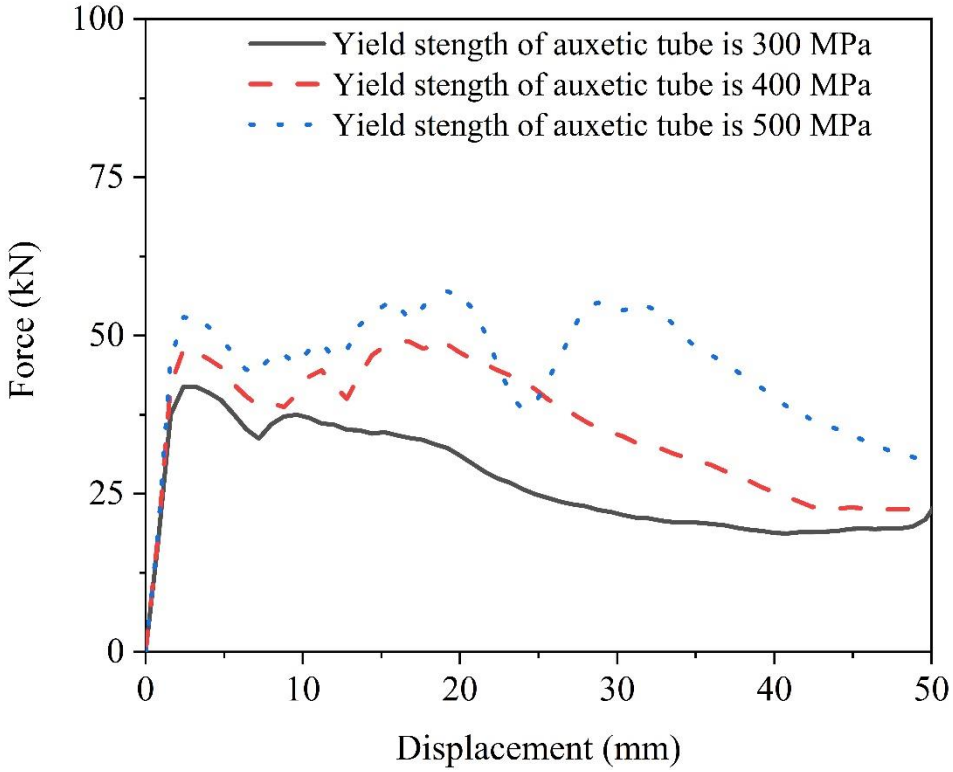

Figure 24. Numerically simulated force-displacement curves of hybrid tube with different yield strengths of the auxetic tube material.

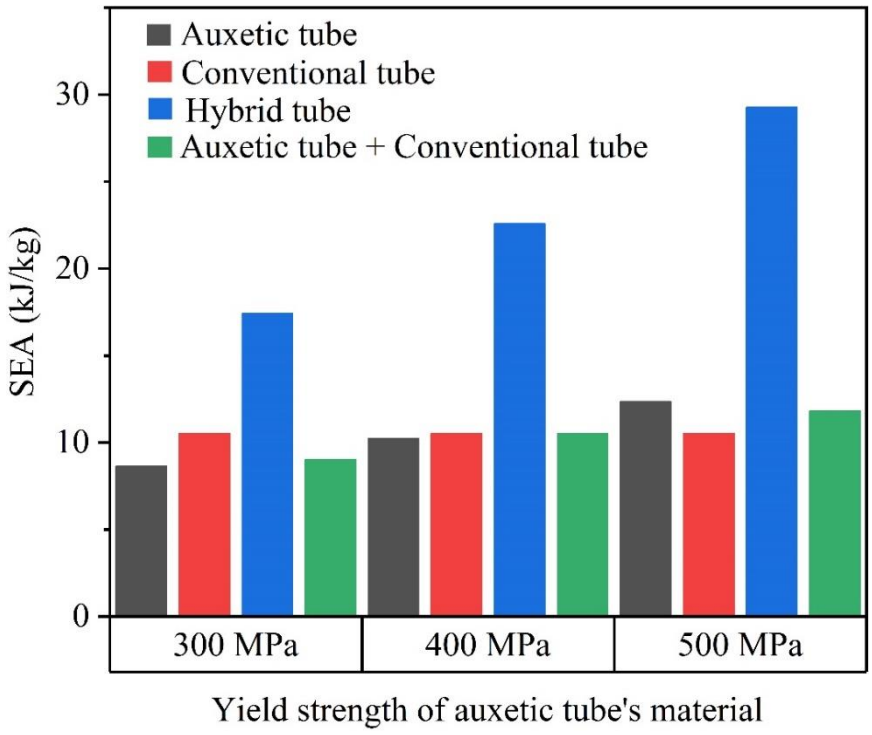

Figure 25. Numerically simulated specific energy absorption of the tubes with different yield strengths of the auxetic tube material. (Note: material used for the conventional tube remains unchanged.)

Table 1. Summary of test types and specimen dimensions (all the specimens were made of AA6060 T5)

Test type	**Specimens**		**Dimensions (mm)**		**Remarks**
			Outer diameter	**Wall thickness**	
Axial compression of tube	Auxetic tube		49.92 ± 0.03	2.74 ± 0.03	Elliptical holes were cut using conventional machining technique.
	Conventional tube		43.87 ± 0.06	1.44 ± 0.01	
	Hybrid tube	Outer auxetic tube	49.92 ± 0.03	2.74 ± 0.03	A small gap exists between the outer auxetic tube and inner conventional tube
		Inner conventional tube	43.87 ± 0.06	1.44 ± 0.01	
Tensile tests of coupons	Flat dog-bone coupons		Please refer to Fig. 3(a).		Coupons were cut from tubes and tested according to AS 1391-2007 to obtain material properties.

Table 2. Averaged dimensions of the elliptical holes cut on the auxetic tubes

	Dimensions	Measured values (averaged)	
		a (mm)	b (mm)
Vertical ellipse	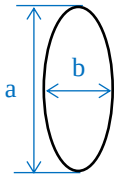	15.68 ± 0.02	6.00 ± 0.03
Horizontal ellipse	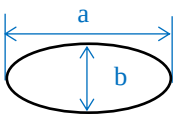	13.56 ± 0.06	6.97 ± 0.02